JACS
JOURNAL OF THE AMERICAN CHEMICAL SOCIETY
Article
pubs.acs.org/JACS

Rational Design of a Photomagnetic Chain: Bridging Single-Molecule Magnets with a Spin-Crossover Complex

Rodica Ababei,[†,‡,§,∥] Céline Pichon,[*,†,‡,⊥] Olivier Roubeau,[#] Yang-Guang Li,[†,‡,▽] Nicolas Bréfuel,[†,‡] Lionel Buisson,[†,‡] Philippe Guionneau,[§,∥] Corine Mathonière,[*,§,∥] and Rodolphe Clérac[*,†,‡]

[†]CNRS, CRPP, UPR 8641, F-33600 Pessac, France
[‡]Univ. Bordeaux, CRPP, UPR 8641, F-33600 Pessac, France
[§]CNRS, ICMCB, UPR 9048, F-33600 Pessac, France
[∥]Univ. Bordeaux, ICMCB, UPR 9048, F-33600 Pessac, France
[#]Instituto de Ciencia de Materiales de Aragón (ICMA), CSIC and Universidad de Zaragoza, Plaza San Francisco s/n, 50009 Zaragoza, Spain

Supporting Information

ABSTRACT: The spin-crossover complex $[Fe(LN_5)(CN)_2]\cdot H_2O$ (**1**, LN_5 = 2,13-dimethyl-3,6,9-12,18-pentaazabicyclo[12.3.1]octadeca-1(18),2,12,14,16-pentaene), reported previously by Nelson et al. in 1986, was reinvestigated, and its structure determined by single crystal X-ray diffraction for the first time. The reaction between $[Mn^{III}(saltmen)(H_2O)]^+$ and this photomagnetic linker yielded the trinuclear molecular complex $[\{Mn(saltmen)\}_2Fe_{HS}(LN_5)(CN)_2](ClO_4)_2\cdot 0.5CH_3OH$ (**2**) and the one-dimensional compound $[\{Mn(saltmen)\}_2Fe_{LS}(LN_5)(CN)_2](ClO_4)_2\cdot 0.5C_4H_{10}O\cdot 0.5H_2O$ (**3**) depending on the addition order of the reagents (HS: High-Spin; LS: Low-Spin). Compound **3** exhibits a wave-shaped chain structure built from the assembly of the trinuclear $[Mn^{III}$-NC-$Fe^{II}]$ motif found in **2**. Static magnetic measurements revealed the existence of antiferromagnetic $Mn^{III}\cdots Fe^{II}$ (Fe^{II} HS, $S = 2$) interactions in the trinuclear entity of **2** via the cyanido bridge leading to an $S_T = 2$ ground state. In the case of **3**, concomitant ferromagnetic and antiferromagnetic exchange interactions are found along the chain due to the presence of two crystallographically independent $\{Mn_2(saltmen)_2\}$ units, which behave differently as shown by the magnetic susceptibility analysis, while the Fe^{II} (LS, $S = 0$) cyanido-bridging moiety is isolating these dinuclear Mn^{III} units. ac susceptibility experiments indicated slow relaxation of the magnetization arising from the ferromagnetically coupled $[Mn_2]$ units ($\tau_0 = 1.1 \times 10^{-7}$ s and $\Delta_{eff}/k_B = 13.9$ K). Optical reflectivity and photomagnetic properties of **1** and **3** have been investigated in detail. These studies reveal that the photomagnetic properties of **1** are kept after its coordination to the acceptor Mn^{III}/saltmen complexes, allowing in **3** to switch "on" and "off" the magnetic interaction between the photoinduced Fe^{II} HS unit ($S = 2$) and the Mn(III) ions. To the best of our knowledge, the compound **3** represents the first example of a coordination network of single-molecule magnets linked by spin-crossover units inducing thermally and photoreversible magnetic and optical properties.

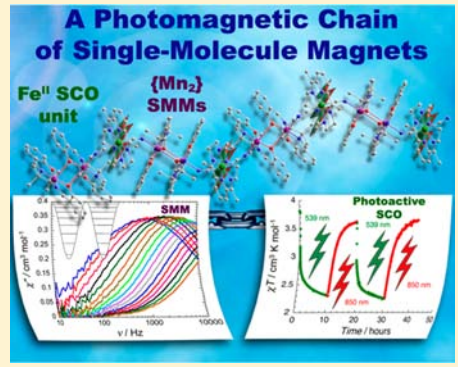

INTRODUCTION

In the field of molecular magnetism, the development of switchable molecule-based materials is spreading since the discovery of bistability of their chemical and physical properties under external stimuli, such as magnetic and electric fields, light, pressure, and temperature.[1] These materials are attracting great attention for both fundamental interests (switching mechanisms) and potential industrial applications (switches, sensors, displays and information storage devices, etc.).[2] The rational design of these molecule-based materials with different dimensionalities (discrete, one- to three-dimensional) is possible thanks to the tools of molecular chemistry offering to chemists a tremendous choice of preformed building blocks with well-defined chemical reactivity and targeted properties (magnetic, optical, conduction, etc.).[3] Single-molecule magnets (SMMs)[4] and single-chain magnets (SCMs)[5,6] are in this context a hot topic since they are showing a magnet behavior at a molecular or one-dimensional (1D) level (i.e., magnetic systems able to keep a magnetization in the absence of an applied magnetic field). These unique systems behave as single domain magnets with slow relaxation of their magnetization below a blocking temperature of the order of 10 K for a time scale of 1 s. Their magnetic bistability is caused and controlled by intrinsic molecular parameters, such as the uniaxial anisotropy, and a high-spin (HS) ground state for the SMMs and also the intrachain interactions for the SCMs. These unique properties make them promising systems to ultimately store information at the molecular level by encoding quantum bits in molecular spins.[7]

Received: July 23, 2013
Published: August 22, 2013

In this research field, recent works have been devoted to the organization of SMMs and SCMs as future applications require a good knowledge of the influence of the magnetic interactions between such molecular magnets on their properties.[8] The crucial effect of the magnetic interactions between SMMs on the quantum tunneling of the magnetization (QTM) was first reported by Wernsdorfer et al. in 2002 in the case of a Mn-based SMM, $[Mn_4O_3Cl_4(O_2CEt)_3(py)_3]$ (S_T = 9/2), paired through hydrogen bonds generating weak antiferromagnetic inter-SMM interactions.[9] Our high interest in this research field was motivated by Wernsdorfer's reports, which demonstrated that modulation of magnetic properties or even new magnetic behaviors are expected for systems incorporating SMMs in magnetic interactions.[9,10] Indeed since these pioneer works, SCMs and SMM-based materials have been designed step by step by association and sometimes coordination of SMMs.[8a,b,d,e] The SMMs bring the necessary uniaxial anisotropy and HS ground state required for the SCM repeating unit, whereas various linkers (diamagnetic or paramagnetic groups, such as organic radicals[11] or metalloligands[5b,12]) are expected to create strong intrachain interactions. In 2002, Miyasaka's team and our group described the first example of a chain incorporating ferromagnetically coupled anisotropic entities.[5b] This initial result led to a family of SCMs $[Mn_2(saltmen)_2Ni(Lao)_2L_2](A)_2$ (saltmen = *N*,*N*′-(1,1,2,2-tetramethylethylene)bis(salicylideneiminate) Scheme 1, Lao = pyridine-2-aldoximate, 1-methylimidazole-2-aldoximate, 1-ethylimidazole-2-aldoximate, and *L* = pyridine, 4-picoline, 4-terbutylpyridine, *N*-methylimidazole; A = $[ClO_4]^-$, $[ReO_4]^-$, $[PF_6]^-$, $[BF_4]^-$, or $[BPh_4]^-$) and initiated a new synthetic strategy to design SCMs using SMM building blocks coupled ferromagnetically in a 1D coordination network.[5b,12] This approach was validated in 2005 connecting the trinuclear $[Mn_2(5\text{-MeO-salen})_2Fe(CN)_6]^-$ SMM unit (5-MeO-salen^{2-} = *N*,*N*′-ethylene bis(5-methoxysalicylideneiminato) dianion) via bis-phenolato bridges to form a chain of the trinuclear {MnFeMn} (S_T = 9/2) repeating motif. As expected, the obtained 1D system, $[NEt_4][Mn_2(5\text{-MeO-salen})_2Fe(CN)_6]$, displays a SCM behavior.[8b] Based on these promising results, an efficient control of the intrachain exchange interaction between the anisotropic or SMM units is a challenge in order to tune at will the magnetic properties of these 1D materials. To control the intrachain magnetic interactions, an appealing approach is to use photomagnetic linkers between SMMs. Among the known photoswitchable molecular species, the spin crossover (SCO) Fe^{II} complexes are certainly the most famous and studied example.[1b,i,2a,13,14] Indeed, many octahedral Fe^{II} complexes are well-known to switch reversibly from a low-spin state (LS, d^6, t_{2g}^6, S = 0) to a HS state (d^6, $t_{2g}^4e_g^2$, S = 2) under a selected light irradiation.[14] This attractive photocontrol of the magnetic properties fueled the research toward a large family of complexes for the construction of switchable molecule-based devices.[1b,i,2a,13d]

Scheme 1

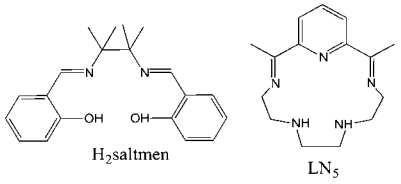

Based on our previous results,[5b,8,11,12] we decided to design photomagnetic chains employing a dinuclear Mn^{III} Schiff-base precursor, $[Mn_2(saltmen)_2]^{2+}$ (S_T = 4),[15] known for its SMM properties and also for its acceptor coordination ability to form an 1D system.[5b,8c,11,12] In order to link this precursor with a SCO building block, the choice of the photomagnetic Fe^{II} complex was dictated mainly by its donor coordination properties and thus by a *trans* position of its potentially coordinating groups. The compounds of general formula $[Fe^{II}(LN_xO_y)(CN)_2]\cdot H_2O$ (LN_5 = 2,13-dimethyl-3,6,9-12,18-pentaazabicyclo[12.3.1]octadeca-1(18),2,12,14,16-pentaene for x = 5 and y = 0, Scheme 1; LN_3O_2 = 3,12,18-triaza-6,9-dioxabicyclo[12.3.1]octadeca-1(18),14,16-triene for x = 3 and y = 2) appeared to be very good candidates to fulfill our requirements.[16] Sato and co-workers have demonstrated in 2005 that the intrinsic photomagnetic behavior of the complex $[Fe(LN_3O_2)(CN)_2]$ is maintained after its coordination in a 1D coordination network.[17] Therefore such *trans*-cyanide complexes are potential building blocks to link SMMs or anisotropic units and thus to obtain unique photoswitchable materials. Recently, Sato et al. and Sutter et al. have respectively observed SMM[18] or SCM[19] behaviors using related $[M(LN_xO_y)]^{2+}$ complexes in cyanido-based compounds. Remarkable solvent-sensitive magnet behaviors were also reported in 3D coordination networks by association of $[Mn(LN_5)]^{n+}$ units with $[Mo(CN)_7]^{4-}$ metalloligands.[20] Finally, it is important to underline that the synthesis of photoactive chains remains a challenge and examples of such systems are rare.[21]

In this work, two new heterometallic compounds based on $[Mn_2(saltmen)_2(H_2O)_2]^{2+}$ and $[Fe(LN_5)(CN)_2]$ building blocks were synthesized and structurally characterized: a discrete trinuclear complex $[\{Mn(saltmen)\}_2Fe(LN_5)(CN)_2](ClO_4)_2\cdot 0.5CH_3OH$ (**2**) and a 1D compound $[\{Mn(saltmen)\}_2Fe(LN_5)(CN)_2](ClO_4)_2\cdot 0.5C_4H_{10}O\cdot 0.5H_2O$ (**3**). Their optical properties studied by reflectivity measurements as well as their magnetic and photomagnetic behaviors have been investigated and discussed in relation with the precursor characteristics. In particular, we are reporting for the first time the crystal structure of the $[Fe_{LS}(LN_5)(CN)_2]\cdot H_2O$ precursor (**1**), together with a detailed reinvestigation of its magnetic, optical, and photomagnetic properties.

EXPERIMENTAL SECTION

Materials and Methods. All experiments were carried out under anaerobic conditions using commercial grade solvent degassed by freeze−pump−thaw technique prior to use. $[Fe(LN_5)(CN)_2]\cdot H_2O$ (**1**) was synthesized according to the procedure described in the literature using Schlenk techniques (see Scheme 1).[16a] For the first time, it was possible to crystallize this Fe^{II} precursor with the following procedure: $[Fe(LN_5)(CN)_2]\cdot H_2O$ (200 mg, 0.53 mmol) was dissolved in MeOH (30 mL) and stirred for 3 h. Insoluble material was removed by filtration. Dark-violet prisms suitable for single crystal X-ray diffraction were obtained by diethyl ether vapor diffusion into the violet solution and filtered quickly after 2 days since the crystals were losing their quality with time. Yield: 16 mg (8%). Anal. calcd for $C_{17}H_{25}FeN_7O$ (399.29 g·mol^{-1}): C 51.14; H 6.31; N 24.56. Found: C 50.48; H 6.33; N 24.11. IR data (KBr, cm^{-1}): $\nu(OH_w)$ 3520 (s), 3372 (s), ν(NH) 3318 (m), 3089 (m), 2902 (s), 2864 (sh), ν(C≡N) 2087 (s), ν(C=N) 1616 (m), 1600 (w), 1563 (w), 1514 (m), 1495 (sh), 1460 (m), 1432 (m), 1395 (m), 1382 (m), 1352 (m), 1312 (s), 1263 (w), 1233 (w), 1204 (m), 1169 (w), 1141 (m), 1080 (w), 1065 (sh), 1033 (s), 973 (w), 937 (w), 913 (sh), 890 (m), 850 (w), 815 (sh), 800 (m), 760 (s), 656 (w), 617 (w). Due the air instability of this Fe^{II} precursor,[16a] its recrystallization and all the reactions with Mn^{III} Schiff-base complexes were done in a glovebox as well as the filtrations and

dx.doi.org/10.1021/ja407570n | J. Am. Chem. Soc. 2013, 135, 14840−14853

Table 1. Summary of the Crystallographic Data for 1−3

	1	2		3	
formula	$C_{17}H_{25}FeN_7O$	$C_{57.5}H_{69}Cl_2FeMn_2N_{11}O_{12.5}$		$C_{59}H_{73}Cl_2FeMn_2N_{11}O_{13}$	
M, g mol^{-1}	399.29	1350.85		1380.91	
crystal system	monoclinic	monoclinic		triclinic	
space group	$P2_1/c$	$P2_1/c$		P-1	
temperature, K	150(2)	150(2)	292(3)	150(2)	298(2)
a, Å	7.643(1)	15.187(3)	15.422(9)	12.730(3)	12.868(3)
b, Å	23.561(5)	30.083(6)	30.744(6)	14.287(3)	14.396(3)
c, Å	10.414(3)	14.054(3)	14.197(9)	18.947(4)	19.151(4)
α, °	90	90	90	87.39(3)	87.04(3)
β, °	102.90(1)	99.04(3)	98.77(2)	76.45(3)	75.62(3)
γ, °	90	90	90	65.67(3)	66.05(3)
V, Å^3	1828.0(7)	6341(2)	6653(1)	3047.5(14)	3135.9(11)
d_{calc}, g cm^{-3}	1.451	1.415		1.505	
Z	4	4		2	
R_1,[a] wR_2[b]	0.0716, 0.1413	0.0611, 0.1717		0.0440, 0.1068	
GOF on F^2	1.020	1.028		1.037	

[a] $R_1 = \sum(||F_o| - |F_c||)/\sum|F_o|$. [b] $wR_2 = [\sum w(F_o^2 - F_c^2)^2/\sum w(F_o^2)^2]^{1/2}$; $w = 1/[\sigma^2(F_0^2) + (aP)^2 + bP]$, where $P = [\max(F_0^2, 0) + 2F_c^2]/3$.

crystallizations. $[Mn_2(saltmen)_2(H_2O)_2](ClO_4)_2$ (see Scheme 1) was prepared according to the previously reported procedure.[15]

Syntheses. *Synthesis of $[Mn_2(saltmen)_2Fe(LN_5)(CN)_2](ClO_4)_2 \cdot 0.5CH_3OH$ (2).* $[Mn_2(saltmen)_2(H_2O)_2](ClO_4)_2$ (0.15 g, 0.15 mmol) dissolved in MeOH (8 mL) was added drop by drop to a methanolic solution (4 mL) of $[Fe(LN_5)(CN)_2]\cdot H_2O$ (0.06 g, 0.15 mmol) in a glovebox. The resulting green solution was stirred for 30 min and filtered. Green crystals suitable for single crystal X-ray diffraction were obtained after 3 days by slow diffusion of diethyl ether into this solution. The crystals were filtered, washed with cold methanol, and dried to air. Yield based on Fe: 100 mg (25%). Anal. calcd for $C_{57.5}H_{69}Cl_2FeMn_2N_{11}O_{12.5}$ (1350.85 g·mol^{-1}): C 51.13; H 5.15; N 11.41. Found: C 50.45; H 5.36; N 10.76. IR data (KBr, cm^{-1}): ν(NH) 3422 (s), 2937 (m), 2885 (sh), ν(C≡N) 2110 (s), ν(C=N) 1602 (s), 1542 (m), 1472 (w), 1442 (m), 1395 (m), 1297 (m), 1207 (w), ν(Cl−O) 1145 (m), 1090 (s), 957 (w), 907 (w), 890 (sh), 847 (w), 817 (w), 800 (w), 767 (m), 627 (m).

Synthesis of $[Mn_2(saltmen)_2Fe(LN_5)(CN)_2](ClO_4)_2 \cdot 0.5C_4H_{10}O \cdot 0.5H_2O$ (3). $[Fe(LN_5)(CN)_2]\cdot H_2O$ (0.2 g, 0.5 mmol) dissolved in MeOH (10 mL) was added drop by drop to a methanolic solution (20 mL) of $[Mn_2(saltmen)_2(H_2O)_2](ClO_4)_2$ (0.5 g, 0.5 mmol) in a glovebox. The resulting dark-brown solution was stirred for 30 min and filtered. Dark-brown crystals suitable for single crystal X-ray diffraction were obtained after 3 days by slow diffusion of diethyl ether into this solution. The crystals were filtered, washed with cold methanol, and dried to air. Yield based on Fe: 1 g (75%). Anal. calcd for $C_{59}H_{73}Cl_2FeMn_2N_{11}O_{13}$ (1380.91 g·mol^{-1}): C 51.32; H 5.33; N 11.16. Found: C 51.90; H 4.99; N 10.56. IR data (KBr, cm^{-1}): ν(NH) 3475 (s), 3242 (w), 2987 (w), 2935 (w), 2875 (w), ν(C≡N) 2080 (s), ν(C=N) 1602 (s), 1547 (m), 1474 (m), 1443 (m), 1396 (m), 1297 (m), 1208 (w), ν(Cl−O) 1151 (sh), 1099 (s), 958 (w), 906 (m), 849 (m), 802 (m), 766 (s), 625 (s).

Crystallography. Single-crystal X-ray crystallographic data of complexes **1**−**3** were collected at 150(2) K on a Nonius Kappa CCD diffractometer with graphite-monochromated Mo K_α radiation (λ = 0.71073 Å). Suitable crystals were affixed on a glass fiber using silicone grease and transferred to the goniometer. DENZO-SMN was used for data integration and SCALEPACK corrected data for Lorentz-polarization effects.[22] The structures were solved by direct methods and refined by a full-matrix least-squares method on F^2 using the SHELXL-97 crystallographic software package.[23] All non hydrogen atoms were refined with anisotropic displacement parameters. Hydrogen atoms were placed geometrically on their carrier atom and refined with a riding model except the hydrogen atoms located on the coordinated N7 and N8 atoms in **2** and **3** found in a difference Fourier map and refined with distance restraints and isotropic displacement parameters derived from their parent atoms (parameters fixed at 1.2 times that of their parent atoms). The hydrogen atoms of the lattice solvent molecules (partial methanol molecules for **2** with occupations of 20 and 30%; water molecule with an occupation of 50% for **3**) could not be found and are omitted in the structural model but taken into account in the formula. In **2**, the perchlorate ions have their oxygen atoms disordered over two positions with relative occupations of 0.76:0.24 and 0.70:0.30 respectively for O11 to O14/O11A to O14A and O21 to O24/O21A to O24A. Displacement parameter restraints were used to refine these disordered moieties as well as part of the macrocyclic ligand (C49 to C55). In **3**, the lattice ether molecule has a 50% occupation, and displacement parameter restraints were used to refine it. Crystal data and structure refinement parameters for complexes **1**−**3** are summarized in Tables 1 and SI1. Selected bond lengths and angles for complexes **1**−**3** are listed in Tables 2 and SI2. Crystallographic data (excluding structure factors) of **1**−**3** have been deposited at the Cambridge Crystallographic Data Centre as supplementary publication nos. CCDC 946651 for **1**, CCDC 946652 for **2**, and CCDC 946653 for **3**. Copies of the data can be obtained free of charge on application to CCDC, 12 Union Road, Cambridge CB21EZ, U.K. (fax: (+44) 1223-336-033; e-mail: deposit@ccdc.cam.ac.uk).

Variable-temperature X-ray high-resolution diffraction patterns were recorded by means of a horizontally mounted INEL cylindrical position-sensitive detector (CPS 120) by gas ionization (argon and ethane) using Debye−Scherrer geometry (angular step 2θ = 0.029°). Monochromatic Cu $K_{\alpha 1}$ radiation was selected as the incident beam.

Physical Measurements. Elemental analyses (C, H and N) were performed following the classical Pregl−Dumas technique on a ThermoFischer Flash EA1112. IR spectra were recorded in the range 4000−400 cm^{-1} on a Nicolet 750 Magna-IR spectrometer using KBr pellets. Magnetic measurements were performed on freshly filtered polycrystalline samples introduced in a polyethylene bag (3 × 0.5 × 0.02 cm) using a Quantum Design SQUID magnetometer (MPMS-XL) and a Quantum Design susceptometer (PPMS) for high-frequency ac experiments. The dc measurements were conducted between 300 and 1.8 K and between −70 kOe and 70 kOe applied dc fields. The thermal dependence of the magnetic susceptibility was measured at 1000 Oe. The field dependences of the magnetization were collected between 1.8 and 8 K, while sweeping the magnetic field between 0 and 7 T at about 100 to 400 Oe/min. The ac susceptibility experiments were realized at ac frequencies ranging from 10 to 10000 Hz with an ac field amplitude of 1 Oe (PPMS) and from 1 to 1500 Hz with an ac field amplitude of 3 Oe (MPMS). Experimental data were corrected for the sample holder and for the diamagnetic contribution of the samples. Photomagnetic experiments were done with a 150 W halogen lamp (LEICA CLS 150X) coupled to an optical fiber directed into the magnetometer cavity. A few milligrams (typically 2−5 mg) of

Table 2. Selected Bond Distances (Å) and Angles (°) for 2 and 3

	2	3
Fe1−C111	2.171(4)	1.924(4)
Fe1−C222	2.182(4)	1.951(4)
Fe1−N5	2.153(5)	1.870(3)
Fe1−N6	2.191(4)	2.081(3)
Fe1−N7	2.318(3)	
Fe1−N8	2.288(4)	2.149(3)
Fe1−N9	2.199(5)	1.915(3)
Mn1−$O1_{eq}$	1.892(3)	1.913(3)
Mn1−$O1_{ax}$		2.545(3)
Mn1−N1	1.986(4)	1.987(3)
Mn1−N2	1.972(4)	1.980(3)
Mn1−$O2_{eq}$	1.865(3)	1.880(2)
Mn2−$O4_{eq}$	1.862(3)	1.887(2)
Mn2−$O4_{ax}$		2.766(3)
Mn2−N3	1.979(4)	1.981(3)
Mn2−N4	1.986(4)	1.985(3)
Mn1−N111	2.150(4)	2.203(3)
Mn2−N222	2.176(4)	2.227(3)
Mn1···Mn1*		3.49
Mn2···Mn2*		3.63
Fe1−C111−N111	174.4(4)	167.8(3)
Fe1−C222−N222	176.1(4)	175.0(3)
Mn1−N111−C111	163.7(3)	147.2(2)
Mn2−N222−C222	160.2(3)	161.2(3)
Mn1−O1−Mn1*		102.1(1)
Mn2−O4−Mn2*		100.9(1)

ground sample were placed into a preformed SQUID straw at a distance of 3 mm from the optical fiber end (the power of the irradiation light was chosen carefully to find a good compromise between minimizing thermal heating of the sample and maximizing the photoconversion efficiency). Sample temperatures were corrected for light-induced heating (average ±2 K at 10 K under white light irradiation), and calibration of experimental sample temperatures was referenced to the data collected in absence of light. Surface reflectivity measurements were performed on a home-built system at different temperatures ranging from 10 to 300 K. The polycrystalline samples were grounded and diluted in $BaSO_4$ prior to any measurements due to the strong absorbance of the materials. Heating and cooling rates were maintained at 4 K min^{-1} during the measurements. This setup collects the light reflected by the sample (sum of direct and diffuse reflected light) that is analyzed by a high-sensitivity Hamamatsu 10083CA spectrometer between 500 and 1000 nm. The spectra are compared to a white reference obtained with a NIST traceable standard for reflectance (SphereOptics, ref SG3054). The background, collected with the light source switched off, is subtracted from all measurements. The reflectivity can be plotted as a function of temperature, time, or wavelength. Different light emitting diodes (LEDs) operating between 385 and 940 nm and bought from Thorlabs were used for excitation measurements. As the samples are potentially very photosensitive, the light exposure time was minimized during all the experiments keeping the samples in the dark except during the spectra measurements when white light is shined on the sample surface (P = 0.4 mW/cm^2). The temperature dependence of the reflectivity spectra was followed during a cycle of cooling−heating. For all the excitation/de-excitation experiments performed at 10 K, the sample was initially placed at this temperature keeping the sample in the dark to avoid any excitation.

RESULTS AND DISCUSSION

Syntheses. $[Fe(LN_5)(CN)_2]\cdot H_2O$ (**1**) was originally synthesized by Nelson et al. in 1986.[16a] This work revealed the existence of two different phases (in methanol) based on elemental analysis, infrared spectroscopy, and thermogravimetric analysis. The authors concluded that the Fe^{II} complex is obtained in its LS state at room temperature from Mössbauer and magnetic data, speculating a six coordinate environment around the Fe^{II} center. Until now, no X-ray crystallographic data were available to confirm this geometry and the molecular structure of this complex. Crystallization conditions under an argon atmosphere of a glovebox were optimized diffusing slowly diethyl ether vapors into a methanolic solution of **1**.[24] Single crystals form after about 2 days, allowing to perform a single crystal X-ray diffraction analysis and to obtain the first crystal structure of **1** (vide infra). It should be mentioned that the obtained crystals are highly air sensitive when they are in their mother solution exposed to air. If the crystals are kept more than 2−3 days in their mother solution, they loose their crystallinity as well as if they are dried. But in the latter case, the obtained powder is not anymore sensitive to oxidation/decomposition based on infrared spectroscopy. Addition of a methanolic solution of $[Mn_2(saltmen)_2(H_2O)_2](ClO_4)_2$ on **1** dissolved in methanol using a 1:1 stoichiometry led to the isolation of a discrete trinuclear compound of formula $[Mn_2(saltmen)_2Fe(LN_5)(CN)_2](ClO_4)_2\cdot 0.5CH_3OH$ (**2**) (Scheme 2). When the same 1:1 reaction is performed adding

Scheme 2

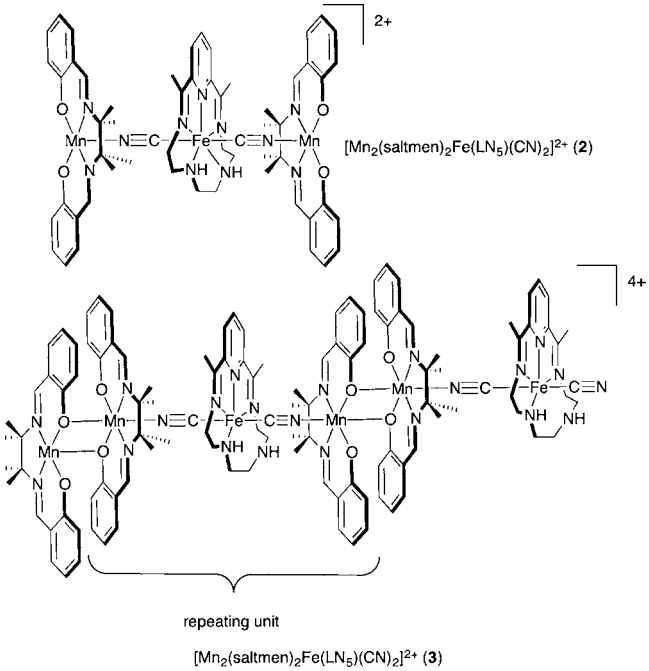

the reagents in the reverse order (i.e., **1** added on the Mn^{III} precursor), the 1D coordination compound $[Mn_2(saltmen)_2Fe(LN_5)(CN)_2](ClO_4)_2\cdot 0.5C_4H_{10}O\cdot 0.5H_2O$ (**3**) was isolated (Scheme 2).

Crystals suitable for X-ray diffraction studies are obtained after 1−4 days by diethyl ether vapor diffusion into the mother solutions. The crystals are stable vs oxidation/decomposition in their mother liquor even in the presence of air. It is also worth noting that the trinuclear complex **2** is the repeating unit of the 1D compound **3**; hence, the synthesis of **3** can be seen as a coordination polymerization of **2**. The infrared spectra (IR) display characteristic: (i) C≡N bands from the macrocyclic

dx.doi.org/10.1021/ja407570n | J. Am. Chem. Soc. 2013, 135, 14840−14853

ligands (1616 cm^{-1} for **1** and 1602 cm^{-1} for **2** − **3**); (ii) Cl−O bands located at 1145 cm^{-1} and 1151 cm^{-1} for **2** and **3**, respectively, indicating the presence of perchlorato anions and confirming the cationic nature of these complexes; and finally (iii) C≡N bands in the 2080−2110 cm^{-1} range: 2087, 2110, and 2080 cm^{-1} for **1**, **2**, and **3** respectively. The C≡N IR bands are known to be extremely sensitive not only to the cyanide coordination to metal centers (to Mn^{III} Schiff-base complexes in our case) but also to the Fe^{II} spin state.[2S,16a] Indeed, cyanide vibration bands of a Fe^{II}/CN complex are lower in energy in its HS spin state than in its LS spin form as exemplified by **1** that is a LS species at room temperature exhibiting a ν_{CN} band at 2087 cm^{-1}. Therefore, the IR spectra of **2** and **3** suggest that they possess Fe^{II} metal ions in their HS (2110 cm^{-1}) and LS (2080 cm^{-1}) states, respectively. The difference in the Fe^{II} spin state is also coherent with the different colors of the crystals (green for **2** and brown for **3**), the Fe^{II} coordination sphere, and the magnetic measurements (vide infra).

Structural Descriptions. *Structure of $[Fe(LN_5)(CN)_2]\cdot H_2O$ (**1**).* When a single crystal of **1** is filtered from the mother liquor and directly mounted on the X-ray diffractometer, the diffraction pattern at 150 K is evolving during the data collection. After roughly 8 h, new diffraction spots are appearing and are not anymore corresponding to the initial unit cell. This structural change is in fact due to a partial loss of interstitial water molecules in the crystal structure. Freshly filtered crystals incorporate 1.125 water molecules in the crystallographic unit cell (see Table SI1); while during the crystallographic collection after roughly 8 h, the last set of X-ray diffraction frames are corresponding to a new phase. A full structural collection revealed that the second phase incorporates only one water molecule disordered over two positions (occupancies of 0.8 and 0.2). This structural conversion induced by the loss of 0.125 water molecule leads to a crystalline rearrangement and a more stable phase defined by a smaller unit cell (volume almost divided by 2).

In the following, the structure of **1** will only be described in its thermodynamic state after filtration as all the physical characterizations were done on this phase. $[Fe(LN_5)(CN)_2]\cdot H_2O$ (**1**) crystallizes in the monoclinic $P2_1/c$ space group. The hexacoordinated Fe^{II} ion (as predicted by Nelson)[16a] is surrounded by four nitrogen atoms from the macrocyclic ligand LN_5 defining the equatorial plane ($Fe-N_{eq}$ = 1.839(4)−2.097(3) Å) and two cyanido ligands in axial positions (Figure 1 and Table SI2). The fifth N(7) atom of the LN_5 ligand is uncoordinated and hanging out of the plane defined by the macrocyclic ligand (dN7-N3/N4/N5/N6 = 1.212 Å). The axial Fe−C bond lengths are equal to 1.948(5) and 1.964(5) Å, and as expected, the C1−Fe1−C2, N1−C1−Fe1, and N2−C2−Fe2 angles are close to the linearity (171.5(2), 175.4(4), and 178.0(4)°, respectively). The coordination sphere and the bond lengths around the Fe^{II} ion are indicative of its LS state as already observed in the $[Fe(LN_3O_2)(CN)_2]\cdot H_2O$ complex.[16c,26] In the crystal structure, the $[Fe(LN_5)(CN)_2]$ complexes are arranged in the (*b*,*c*) plane in a 1D supramolecular network (Figure SI1). The water molecules connect the Fe^{II} complexes via hydrogen bonds occurring between the cocrystallized water molecule and the terminal nitrogen atoms from the CN groups (shortest hydrogen interaction $O_w\cdots N$ = 2.84 Å). No additional phase evolution, transition, or degradation was detected with time or temperature as evidenced by powder X-ray diffraction patterns recorded between 110 and 370 K (Figure SI2). This monohydrated phase is thus thermally stable after filtration up to 370 K, and no indication of structural change or phase transition was detected that could indicate a spin-crossover phenomenon.

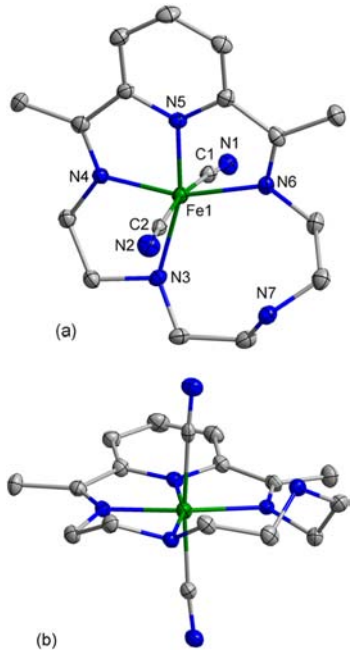

Figure 1. ORTEP-type views of $[Fe(LN_5)(CN)_2]$ in the crystal structure of **1** with thermal ellipsoids fixed at 30% (a, top and b, side views). Fe, N, and C atoms are indicated in green, blue, and gray, respectively, while hydrogen atoms and water molecules are omitted for clarity.

*Structure of $[\{Mn(saltmen)\}_2Fe(LN_5)(CN)_2](ClO_4)_2\cdot 0.5CH_3OH$ (**2**).* Compound **2** crystallizes in the monoclinic $P2_1/c$ space group as a trinuclear complex constituted of two $[Mn(saltmen)]^+$ moieties bridged by one $[Fe^{II}(LN_5)(CN)_2]$ unit. The Fe^{II} metal ion is now heptacoordinated by the five nitrogen atoms of the macrocyclic LN_5 ligand (d_{Fe-N} = 2.153(5)−2.318(3) Å) and two axial cyanido groups (d_{Fe-C} = 2.171(4)−2.182(4) Å). These Fe−X (X = N or C) bond lengths and the heptacoordinence are characteristic of a HS Fe^{II} ion.[16c,26,27] It should be emphasized that the $[Fe(LN_5)(CN)_2]$ species is for the first time observed in its HS state, whereas **1** crystallized in its LS state.

Both Mn^{III} sites are pentacoordinated with a square pyramidal geometry. Their equatorial planes are defined by two nitrogen and two oxygen atoms from the $saltmen^{2-}$ ligand ($d_{Mn-N/O}$ = 1.865(3)−1.986(4) Å, see Table 2). The Mn^{III} axial positions are occupied by terminal nitrogen atoms of the cyanido groups from the $[Fe^{II}_{HS}(LN_5)(CN)_2]$ moiety (d_{Mn-N} = 2.150(4) and 2.176(4) Å). The Fe−C−N angles are close to linearity (174.4(4) and 176.1(4)°), while the Mn−N−C angles equal to 160.2(3) and 163.7(3)° are responsible of the bent shape of the trinuclear complex (Figure 2). The intramolecular Mn···Fe distances are equal to 5.38 and 5.41 Å. In the crystal packing along the *a* axis, the trinuclear complexes are associated in supramolecular double chains through weak van de Waals interactions without significant π stacking interactions (the shortest centroid to centroid distance is ∼4.14 Å, Figure SI3a). These two parallel chains of trinuclear complexes are arranged in layers separated by ClO_4^- ions (Figure SI3b). The shortest intercomplex Mn···Mn, Fe···Fe, and Mn···Fe distances are 7.38,

dx.doi.org/10.1021/ja407570n | J. Am. Chem. Soc. 2013, 135, 14840−14853

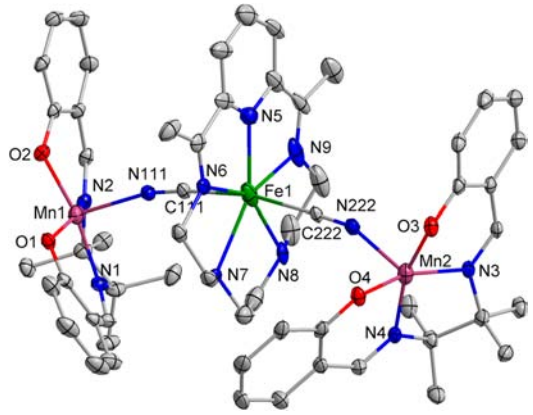

Figure 2. ORTEP-type view of the $[Mn_2(saltmen)_2Fe(LN_5)(CN)_2]^{2+}$ cation in the crystal structure of **2** with thermal ellipsoids fixed at 30%. Mn, Fe, N, O, and C atoms are indicated in purple, green, blue, red, and gray, respectively, while hydrogen atoms, perchlorate anions, and interstitial methanol molecules are omitted for clarity.

8.12, and 8.49 Å. At 292 K, the unit cell of **2** was checked and found to be very similar to 150 K (Tables 1 and SI1).

*Structure of [{Mn(saltmen)}$_2${Fe(LN$_5$)(CN)$_2$}](ClO$_4$)$_2$·0.5C$_4$H$_{10}$O·0.5H$_2$O (**3**).* Complex **3** crystallizes in the triclinic *P*-1 space group. The unit cell contains the cationic trinuclear $[\{Mn(saltmen)\}_2\{Fe(LN_5)(CN)_2\}]^{2+}$ unit, two perchlorato counter-anions and disordered ether and water solvent molecules. The cationic $[\{Mn(saltmen)\}_2Fe(LN_5)(CN)_2]^{2+}$ moiety includes two $[Mn^{III}(saltmen)]^+$ cations connected by the neutral $[Fe^{II}(LN_5)(CN)_2]$ linker (Figure 3a) as observed in **2**. However in contrast to complex **2**, the Mn^{III} sites are hexacoordinated in **3**. Oxygen atoms from phenolato groups of neighboring trinuclear units are coordinated to the Mn^{III} axial positions, resulting in dinuclear $[Mn_2(saltmen)_2]^{2+}$ moieties and the 1D coordination network. In the dinuclear $\{Mn^{III}_2\}$ components, both Mn^{III} centers are surrounded by two N and two O atoms of the saltmen ligand in the equatorial plane, one axial N atom derived from a $[Fe^{II}(LN_5)(CN)_2]$ unit and one axial oxygen atom coming from a phenolato group of an adjacent $[Mn^{III}(saltmen)]^+$ unit. Based on the aforementioned metal ion coordinations, the $[Mn_2(saltmen)_2]^{2+}$ and $[Fe^{II}LN_5(CN)_2]$ units are connected via Mn^{III}–N–C–Fe^{II} bridges into a wave-shaped chain running along the $b + c$ direction (see Figures 3b and SI4). Two non equivalent manganese sites are present in the asymmetric unit; hence, the chain contains two non equivalent $[Mn_2(saltmen)_2]^{2+}$ units. This structural feature will have a great importance on the discussion of the magnetic behavior of **3** (vide infra). In the equatorial plane of the Mn^{III} sites, the Mn1–X (X = N or O atom of the saltmen ligand) and Mn2–X average bond lengths are 1.94 and 1.93 Å, respectively (see Table 2). As usually observed for octahedral Mn^{III} ions, the Jahn–Teller distortion leads to elongated axial Mn–N_{cyano} and Mn–$O_{saltmen}$ bonds (2.203(3) and 2.545(3) Å for Mn1; 2.227(3) and 2.766(3) Å for Mn2) that are significantly longer for the Mn–O bonds than those observed in the $[Mn_2(saltmen)_2(H_2O)_2](ClO_4)_2$ precursor.[15a] The $Mn^{III}\cdots Mn^{III}$ distances in the $\{Mn^{III}_2\}$ moieties are 3.49 and 3.63 Å, while the Mn–O–Mn angles are 102.1(1) and 100.9(1)°, respectively (see Table 2).

In the $[Fe(LN_5)(CN)_2]$ fragment, the Fe^{II} center is hexacoordinated with four N atoms from the LN_5 ligand and two C atoms from the cyanido groups. The Fe–N bond lengths are in the range of 1.870(3)–2.149(3) Å, whereas the Fe–C bond lengths are equal to 1.924(4) and 1.951(4) Å (see Table 2). The Fe–C/N bond lengths are similar to those found for the LS $[Fe^{II}(LN_5)(CN)_2]$ precursor suggesting that the Fe1 site is in its LS state as also confirmed by infrared spectroscopy.

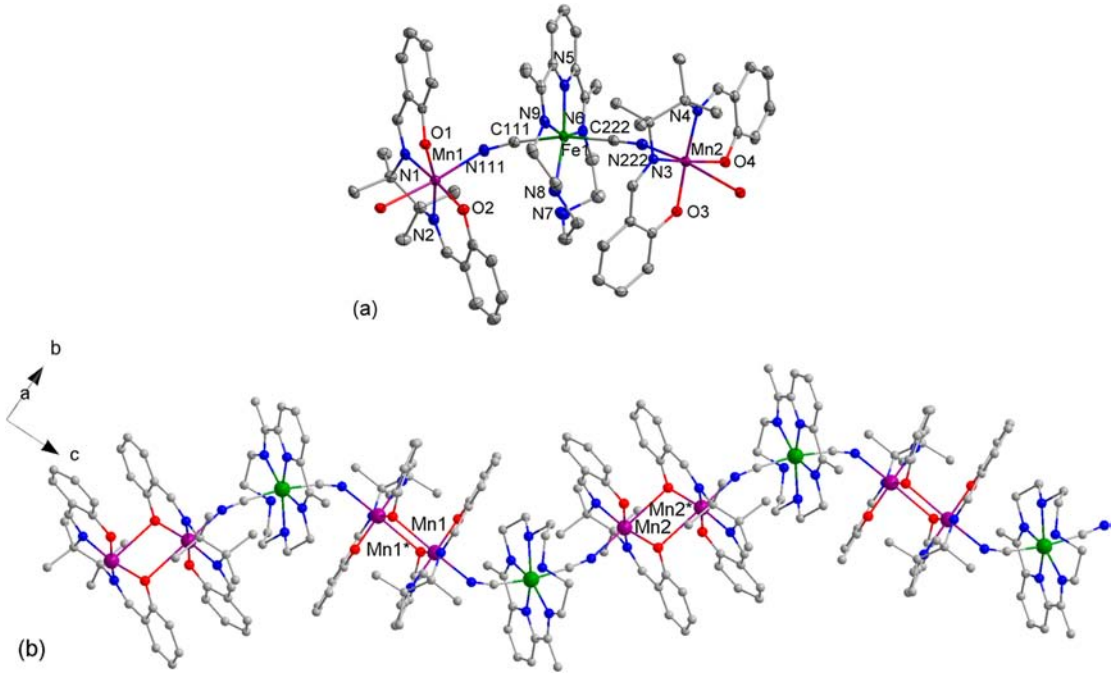

Figure 3. (a) ORTEP-type representation of the asymmetric unit of **3** with thermal ellipsoids fixed at 30% and (b) ball-and-stick representation of the coordination chain, $[Mn_2(saltmen)_2Fe(LN_5)(CN)_2]^{2+}$, in **3** recorded at 150 K with symmetry operators for the generated atoms: * = $-x, -y, -z$. Mn, Fe, N, O and C atoms are indicated in purple, green, blue, red, and gray, respectively, while hydrogen atoms, perchlorate anions, and interstitial solvent molecules are omitted for clarity.

dx.doi.org/10.1021/ja407570n | J. Am. Chem. Soc. 2013, 135, 14840–14853

The Mn1−N111−C111 and Fe1−C111−N111 bond angles are 147.2(2) and 167.8(3)°, while Mn2−N222−C222 and Fe1−C222−N222 are 161.2(3) and 175.0(3)°, respectively (see Table 2). These angles, strongly deviating from linearity, are responsible of the wave shape of the chain. The intrachain $Mn^{III}\cdots Fe^{II}$ distances are ca. 4.95 Å and 5.24 Å. In the crystal structure, the chains are forming supramolecular layers in the (*b*,*c*) plane interacting through π stacking between phenyl rings of the saltmen ligand and of the LN_5 ligand (centroid to centroid distance of 3.80 Å, Figure SI4). These chain layers are separated by ClO_4^- counterions, diethyl ether and water molecules (Figures SI5). The shortest Mn···Mn distance between two planes is ∼14.29 Å. At 298 K, the unit cell of **3** was checked and found to be very similar to that at 150 K (Tables 1 and SI1).

The $[Fe(LN_3O_2)(CN)_2]$ fragment is known to adopt a hexa- or a hepta-coordinated environments in its LS and HS states, respectively.[16,27] The $[Fe(LN_5)(CN)_2]$ derivative is also hexacoordinated in its LS state,[28] while an heptacoordinated geometry is predicted for its HS form.[16a] Therefore the structural analysis of the present compounds suggests that the Fe^{II} site in **1** and **3** is in its diamagnetic LS state, while in **2**, it exhibits a HS state. The magnetic properties of these compounds have been performed to confirm this conclusion and to detect any possible spin-crossover phenomenon and/or photoactivity.

Magnetic Properties. The magnetic susceptibility of **1**−**3** have been measured on polycrystalline samples using dc and ac techniques. The dc magnetic properties are presented as χT vs T plots (χ being the molar susceptibility defined as M/H per formula unit, see Table 1). In agreement with the previous results obtained by Sánchez-Costa et al.,[28] **1** is diamagnetic over the whole temperature range (up to 350 K) with a χT value very close to zero (Figure SI6, red points). Temperature dependences of the χT product of **2** and **3** are displayed Figure 4. At 300 K, the χT product of **2** and **3** is respectively equal to

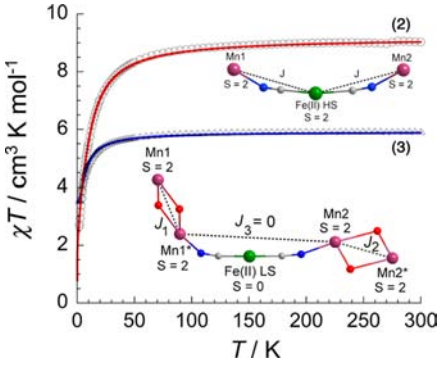

Figure 4. Temperature dependence of the χT product for **2** and **3** at 1000 Oe. The solid lines indicate the best fits obtained with the isotropic Heisenberg magnetic model described in the text. Inset: Schemes of the spin and magnetic interaction topologies in **2** and **3**.

9.0 and 5.9 cm^3 K mol^{-1}, which is in good agreement with the theoretical Curie constants expected to be 9 and 6 cm^3 K mol^{-1}, respectively, for two Mn^{III} ions (HS, $S_{Mn} = 2$) and one Fe^{II} ion (HS state with $S_{Fe} = 2$ for **2** and LS state with $S_{Fe} = 0$ for **3**). As already discussed in the X-ray structure analysis (vide supra), both compounds are indeed constituted of the same repeating unit of $\{Mn_2Fe\}$ formula although with a Fe^{II} center in different spin state. Lowering the temperature, the χT products are slowly decreasing until 50 K before rapidly dropping to reach 2.65 and 3.55 cm^3 K mol^{-1} at 1.8 K, respectively, for **2** and **3**. This thermal behavior is typical of dominant antiferromagnetic interactions between paramagnetic centers that are probably reinforced below 10 K by the influence of magnetic anisotropy, intermolecular (for **2**) and interchain (for **3**) antiferromagnetic interactions. In order to quantify the magnetic interaction between Mn^{III} and Fe^{II} ions in the trinuclear complex **2**, the following isotropic Heisenberg Hamiltonian (eq 1) has been used:

$$H = -2J(S_{Mn1}\cdot S_{Fe} + S_{Fe}\cdot S_{Mn2}) \quad (1)$$

with $S_{Mn1} = S_{Mn2} = 2$, $S_{Fe} = 2$, and J being the average Mn^{III}–Fe^{II} magnetic interaction through the cyanido bridge.

The analytical expression of the susceptibility (eq 2) was deduced from the Van Vleck equation[29] in the weak-field limit ($k_BT \gg g\mu_BH$):

$$\chi_{tot} = \frac{Ng^2\mu_B{}^2}{3k_BT}\cdot\frac{A}{B} \quad (2)$$

with $A = 6(5 + \exp(4x) + 14\exp(6x) + 5\exp(8x) + \exp(10x) + 50\exp(14x) + 5\exp(18x) + 19\exp(20x) + 30\exp(22x) + 69\exp(24x) + 30\exp(28x) + 55\exp(32x) + 91\exp(36x))$; $B = 5 + 3\exp(4x) + 7\exp(6x) + 6\exp(8x) + 3\exp(10x) + 24\exp(14x) + 5\exp(18x) + 12\exp(20x) + 9\exp(22x) + 18\exp(24x) + 9\exp(28x) + 11\exp(32x) + 13\exp(36x)$; and $x = J/k_BT$.

This Heisenberg model leads to a fit of very good quality down to 1.8 K (Figure 4, red line) obtained with the following set of parameters: $J/k_B = -0.96(3)$ K and $g = 2.02(5)$.

The sign of J confirms the antiferromagnetic interaction between Mn^{III} and Fe^{II} ions in the trinuclear complex **2**, stabilizing an $S_T = 2$ ground state, although the corresponding plateau is not reached at the lowest accessible temperature. As far as we know, **2** is the first Fe^{II}_{HS}–CN–Mn^{III}_{HS} system allowing the estimation of the Fe^{II}_{HS}–Mn^{III}_{HS} magnetic interaction through the cyanido bridge. In addition, magnetic models including single-ion magnetic anisotropy (defined by the following Hamiltonian of anisotropy: $H_A = 2D_{Mn}S_{Mn,z}{}^2 + D_{Fe}S_{Fe,z}{}^2$) and/or intercomplex magnetic interactions were also tested, but they do not improve significantly the quality of the χT vs T fit and do not modify the obtained J value (−0.96(3) K). Nevertheless, the addition of the magnetic anisotropy in the magnetic analysis allows to simulate qualitatively well both the χT vs T and M vs H data below 8 K (Figure SI7) with $D_{Mn}/k_B = -4.6(5)$ K and $D_{Fe}/k_B = +0.8(1)$ K (keeping fixed the other parameters: $J/k_B = -0.96$ K and $g = 2.02$). It is important to consider the values of the single-ion anisotropy parameters as a qualitative estimation, as they might also contain phenomenologically the contributions from other magnetic parameters, such as the intercomplex interactions.

In the case of **3**, the analysis of the experimental data is more complicated as two non equivalent $\{Mn_2\}$ units are linked by the diamagnetic $[Fe^{II}(LN_5)(CN)_2]$ entity. In a first approximation, only the exchange interactions between Mn^{III} ions were taken into account in the magnetic model considering negligible the interaction through the diamagnetic Fe^{II}_{LS} unit. The corresponding isotropic Heisenberg Hamiltonian is given by eq 3:

$$H = -2J_1(S_{Mn1}\cdot S_{Mn1*}) - 2J_2(S_{Mn2}\cdot S_{Mn2*}) \quad (3)$$

dx.doi.org/10.1021/ja407570n | J. Am. Chem. Soc. 2013, 135, 14840−14853

with $S_{Mn1} = S_{Mn1*} = S_{Mn2} = S_{Mn2*} = 2$ and J_1 and J_2 being the two Mn^{III}–Mn^{III} magnetic interaction through the bisphenolato bridge. The expression of the magnetic susceptibility was deduced from the Van Vleck expression[29] in the weak field limit ($k_BT \gg g\mu_BH$):

$$\chi_{tot} = \frac{Ng^2\mu_B^2}{k_BT}(\chi_1 + \chi_2)/2 \quad (4)$$

with $\chi_i = (2\exp(2x_i) + 10\exp(6x_i) + 28\exp(12x_i) + 60\exp(20x_i))/(1 + 3\exp(2x_i) + 5\exp(6x_i) + 7\exp(12x_i) + 9\exp(20x_i))$ and $x_i = J_i/k_BT$.

It should be first noted that it is impossible to fit the experimental data (even qualitatively) if the $\{Mn_2\}$ units are considered as identical ($J_1 = J_2$). Only when $J_1 \neq J_2$, a very good agreement between the model and the experience is obtained (Figures 4 and SI8), leading to the following parameters: $J_1/k_B = -1.09(9)$ K, $J_2/k_B = +0.04(1)$ K, and $g = 2.00(5)$. This result confirms the presence of a dominant antiferromagnetic interaction in one of the dinuclear Mn^{III} unit, while a weak ferromagnetic coupling is detected in the second one. Most of the dinuclear Mn^{III} Schiff-base complexes bridged through bisphenolato groups reported in the literature[15,30−32] display intramolecular ferromagnetic interactions[15,32] resulting in some cases to SMM behavior induced by their $S_T = 4$ ground state and the magnetic anisotropy of the Mn^{III} ions.[15b,32] Nevertheless, examples of antiferromagnetically coupled Mn^{III} Schiff-base complexes have also been reported,[30,31,32d] and thus it is not surprising to observe both types of species coexisting in **3**. Unfortunately the magnetostructural correlation ($Mn-O_{eq}$ bond distance vs J) previously reported for a $\{Mn^{III}_2\}$ family of saltmen-derivative compounds does not seem to apply in the present case probably due to the large difference in the other geometric parameters and in particular the Mn−O−Mn* angle (Mn1−O1−Mn1* = 102.1(1); Mn2−O4−Mn2* = 100.9(1)°).[15] On the basis of the $Mn-O_{ax}$ bond distances ($Mn1-O1_{ax} = 2.545(3)$ Å and $Mn2-O2_{ax} = 2.766(3)$ Å) and Mn−O−Mn* angles, similar dinuclear complexes can be identified in refs 15 and 30, suggesting that the $\{Mn1_2\}$ and $\{Mn2_2\}$ units are respectively antiferromagnetically and ferromagnetically coupled.

To further confirm this magnetic model, the susceptibility of a classical $S = 2$ spin chain (including J_1, J_2, and the Mn^{III}–Mn^{III} interaction, J_3, via the diamagnetic $[Fe^{II}(LN_5)(CN)_2]$ pathway) has been calculated on the basis of Fisher's work.[33] The fit of the experimental data ($J_1/k_B = -1.13(5)$ K, $J_2/k_B = +0.03(1)$ K, $J_3/k_B = -0.00008(6)$ K, and $g = 2.00(5)$) is virtually identical to the previous one shown in Figure 4 confirming the former analysis and the negligible contribution of the exchange coupling mediated by the diamagnetic Fe^{II} complex. It is important to mention that a more elaborated magnetic model (with $J_3 = 0$) including magnetic anisotropy on the two Mn^{III} sites does not improve the χT vs T fit. The obtained J values are not significantly altered, but it is still not possible to obtain a satisfactory modeling of the M vs H data below 10 K (Figure SI9) probably due to the misalignment of the local easy magnetic axis (Jahn−Teller axis) on the different Mn^{III} ions.

To summarize, **3** is a 1D coordination compound constituted of two magnetically isolated dinuclear units with different spin ground state $S_T = 0$ and $S_T = 4$ induced by antiferromagnetic and ferromagnetic intraunit interactions, respectively. As already observed for related Mn^{III}/salen-type complexes,[15b,32] slow relaxation of the magnetization, i.e., SMM properties, could be observed for the $S_T = 4$ $\{Mn^{III}_2\}$ moiety in **3**. Therefore the dynamic properties of **3** were studied by ac susceptibility measurements in zero dc field under variable frequencies (10−10000 Hz) and temperatures ranging from 1.8 to 5 K (Figure SI10). Both in-phase (χ') and out-of-phase (χ'') components of the ac susceptibility appear to be frequency and temperature dependent (Figure SI10), indicating the presence of slow relaxation of the magnetization in **3**. In zero dc field, the characteristic frequencies and temperatures of the dynamics can not be determined, as no maximum of the χ'' signal is observed in the experimental temperature and frequency windows. In other words, the relaxation process is too fast at zero dc field to determine its characteristic time (τ). As quantum tunneling of the magnetization (QTM) might be an effective pathway of relaxation above 1.8 K, additional ac susceptibility measurements were performed under weak dc fields, which should lift the $\pm m_S$ energy level degeneracy and thus lower the probability of QTM. These ac measurements were performed in various dc fields ranging from 0 to 10000 Oe. As shown in Figures SI11 and SI12, the relaxation is slowed down, as expected lowering the probability of QTM, and the maximum on the χ'' vs ν data is shifted at frequencies below 1500 Hz for magnetic fields between 700 and 3500 Oe. After estimating the optimum dc field at 1400 Oe from the $\nu_{max} = f(H)$ plot (Figure SI12), ac measurements were performed under 1400 Oe dc field (Figures 5 and SI13).

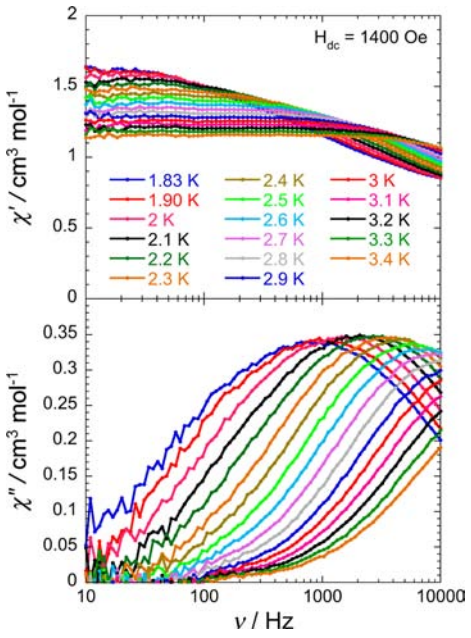

Figure 5. Frequency dependence of the in-phase (top, χ') and out-of-phase (bottom, χ'') susceptibility recorded on a polycrystalline sample of **3** at different temperatures between 1.83 and 3.4 K with an applied dc field of 1400 Oe.

Below 4 K, the in- and out-of-phase ac susceptibilities are found to be strongly dependent on the ac frequency with a single relaxation mode observed on the χ'' vs ν data. Using the maxima of the χ'' signals, the relaxation time ($\tau = 1/(2\pi\nu_{max})$) of **3** was estimated as a function of the temperature (Figure 6).

The relaxation time is thermally activated following an Arrhenius law (eq 5) with $\Delta_{eff}/k_B = 13.9$ K and $\tau_0 = 1.1 \times 10^{-7}$ s (with τ_0 and Δ_{eff} being respectively the preexponential factor

dx.doi.org/10.1021/ja407570n | J. Am. Chem. Soc. 2013, 135, 14840−14853

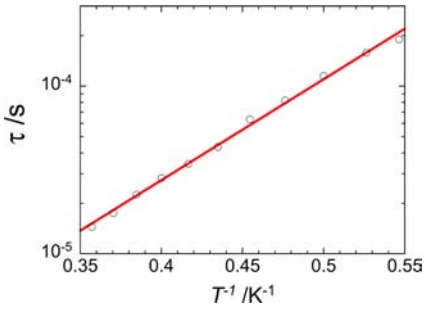

Figure 6. Temperature dependence of the relaxation time (τ) plotted as τ vs $1/T$ for **3** deduced from ac measurements at 1400 Oe (Figure 5 and SI13). The red solid line corresponds to the least-squares fit of the data to an Arrhenius law (see parameters indicated in the text).

of the Arrhenius law and the energy barrier to reverse the magnetization).

$$\tau = \tau_0 \exp(\Delta_{eff}/k_B T) \quad (5)$$

The obtained Δ_{eff} value falls within the usual range (15−20 K) found for isolated $S_T = 4$ $\{Mn^{III}_2\}$/Schiff-base SMMs.[15b,32b−f,34] This result shows that **3** behaves on a magnetic point of view as an isolated SMM due to the presence of $S_T = 4$ $\{Mn^{III}_2\}$ unit in the 1D coordination network.

Optical Reflectivity and Photomagnetic Properties. This paragraph is mainly devoted to the optical and photomagnetic behaviors of **3** as this compound contains LS $[Fe^{II}(LN_5)(CN)_2]$ moieties that are potentially photoactive. For comparison, the detailed properties of the crystalline complex **1** are also described in relation with published studies on powder samples.[28] To be exhaustive, the optical properties of **2** were also studied. As expected in presence of a HS Fe^{II} and $S = 2$ Mn^{III}/salen moieties,[35] the absolute reflectivity of **2** shows only a weak thermochromism in the 10−300 K temperature range (Figure SI14).

The reflectivity spectra of **1** is only slightly temperature dependent (Figure SI15a). This weak thermochromism is better seen when plotting the temperature dependence of the absolute reflectivity at 800 nm, noted R_{800}, in the dark (Figure SI15b). Limited changes of the spectrum are observed in agreement with an $S = 0$ spin state in the whole experimental temperature range. Nevertheless, a small variation of R_{800} with a thermal hysteresis effect is observed below 120 K as a signature of the photoinduced SCO (photoinduced conversion of LS into HS species). This result emphasizes the strong sensitivity of **1** to the light irradiation as the light exposure time of the sample was reduced to the minimum required to collect spectra. These thermally and photoinduced behaviors are in agreement with the known spin-crossover phenomenon reported for powder samples of **1**.[28] In order to establish the time needed to fully populate the HS state at 10 K, the sample was irradiated with a white light ($P = 0.4$ mW/cm^2) during 90 min. Indeed in less than 30 min, the spectrum does not change anymore (Figure SI15c), and R_{800} is quasi-saturated after only 20 min (Figure SI15c inset). The thermal stability of the photoinduced HS phase was also probed increasing the temperature (at 4 K/min, Figure SI15d). The R_{800} reflectivity signal starts to increase around 120 K until recovering the typical values of the LS state above 160 K. These results obtained under white light irradiation are similar to those reported by Sánchez-Costa et al.[28] In order to fully characterize the metastable photoinduced HS state, additional photoexcitation experiments were performed at selected wavelengths ranging from 940 to 385 nm (±10 nm) using LED sources. The optimal wavelength to photoconvert the LS state was determined by checking the efficiency of the different LEDs in similar conditions at 10 K: 5 min of irradiation at a power of 0.8 mW/cm^2 (before each excitation, the sample was heated to 160 K and cooled down to 10 K in complete dark to fully relax the photogenerated HS sites). The plot of the difference between the absolute reflectivity before and after LED irradiation at 800 nm, $\Delta R = R_{after} - R_{before}$, as a function of the LED wavelength (Figure SI16a) reveals the most efficient wavelength at 455 nm. But it is important to notice that a broad domain of light excitations between 625 and 385 nm is indeed efficient, explaining why the HS state can be easily populated with a white light irradiation (Figures SI15). As expected, the fact that the HS phase is photoinduced by a white light or by a 455-nm LED does not change its characteristics (Figures SI16b and SI16c).

The possibility to reverse the LS-to-HS 455-nm photoconversion with another wavelength was also explored even if this effect was previously reported only for the $[Fe(LN_3O_2)(CN)_2]$ analogue.[36] To test this possibility, a crystalline sample of **1** was excited at 10 K and 455 nm (15 min; $P = 1.6$ mW/cm^2) and a second irradiation (5 min; $P = 1.6$ mW/cm^2) at particular wavelengths between 940 and 385 nm was performed. A partial HS-to-LS reverse photoconversion was observed on a broad wavelength domain between 735 and 940 nm (Figures SI17). The initial spectrum of **1** at 10 K (in its diamagnetic state prior to any light exposure) is compared Figure SI17b with the spectra obtained after an 15 min excitation at 455 nm (in its photoinduced HS state) and after a second irradiation at 780 nm done to de-excite the HS state. The two last spectra are almost superposed above 650 nm, while a significant difference is observed around 550 nm (Figure SI17b). This comparison suggests a weak photoreverse effect in **1** that is confirmed by the photomagnetic studies (vide infra).

The photomagnetic properties of **1** were studied in its crystalline form. As anticipated, the paramagnetic HS state can be photoinduced at 10 K as evidenced by the increase of the χT product under irradiations (with white light, 385, 460, or 539-nm LEDs) up to a value around 3 cm^3 K/mol expected for an $S = 2$ species (Figure SI6a). This metastable HS state relaxes around 120 K to the diamagnetic LS thermodynamic state in agreement with the previous relaxation studies.[28] Quite interestingly and as already suggested by the optical reflectivity measurements, a LS-to-HS 460-nm photoconversion (1 h; 15 mW/cm^2) was able to be partially (∼50%) reversed at 10 K using a 950-nm irradiation (15 h; 15 mW/cm^2; Figure SI6b). As far as we know, this result on a crystalline sample of **1** is the first evidence of a photoreversible spin-crossover (even partial) for this system.

In **3**, the Fe^{II} site is hexacoordinated by the LN_5 ligand and the cyanido groups indicating its LS state in the whole temperature range as confirmed by the magnetic measurements (vide supra). Therefore it is natural to expect that the $[Fe^{II}(LN_5)(CN)_2]$ moieties in **3** exhibits optical and photomagnetic properties similar to **1**. The reflectivity spectra recorded in the dark (Figure SI18a) remain quasi-unchanged upon cooling the sample from 270 to 10 K in agreement with the LS Fe^{II} sites. This absence of thermochromism is also seen Figure 7a, on the temperature dependence of the absolute reflectivity at 750 nm (R_{750}) during a complete thermal cycle (cooling and heating modes in the dark). Between 270 and 60

dx.doi.org/10.1021/ja407570n | J. Am. Chem. Soc. 2013, 135, 14840−14853

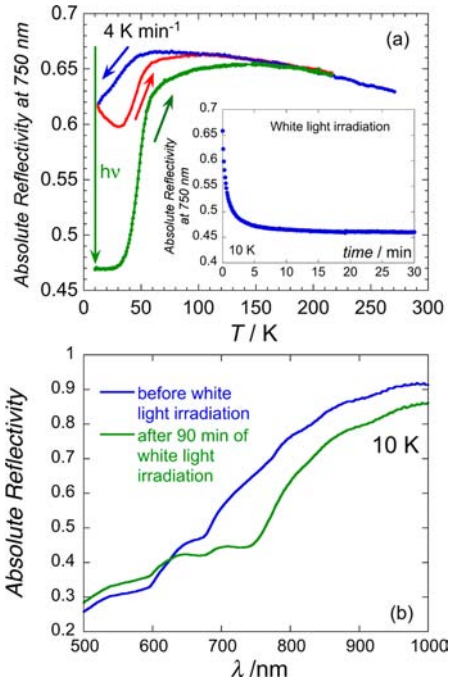

Figure 7. (a) Temperature dependence of the optical reflectivity (with a white spectroscopic light, P = 0.4 mW/cm^2) at 750 nm (R_{750}) of **3** between 270 and 10 K in the dark in cooling (blue) and heating (red) modes and after an exposure to white light (90 min; P = 0.4 mW/cm^2) at 10 K (green). Inset: Time evolution of R_{750} under white light irradiation (P = 0.4 mW/cm^2) at 10 K. (b) Optical reflectivity spectra recorded at 10 K before (blue) and after (green) photoirradiation with white light (90 min; P = 0.4 mW/cm^2).

K, R_{750} (blue symbols) increases slightly from 0.63 to 0.67 (i.e., the absorbance decreases) and only below 50 K a marked decrease of R_{750} is observed as a possible signature of the photoinduced formation of HS $[Fe^{II}(LN_5)(CN)_2]$ moieties under the spectroscopic white light (P = 0.4 mW/cm^2) as already observed for **1** (Figure SI15b). The presence of thermal hysteresis effect between 10 and 100 K (Figure 7a, red and blue symbols) reinforces this hypothesis. To follow the photoexcitation of **3**, the sample was cooled down in the dark at 10 K and then exposed to a constant white light (P = 0.4 mW/cm^2). At 10 K, the optical reflectivity at 750 nm (R_{750}) was monitored in time (Figure 7a inset). In less than 30 min, R_{750} is almost saturated to a much lower value of reflectivity (0.46) as already seen for **1** when the HS state is photogenerated (Figures SI15c and SI15d). The spectacular effect of the white light irradiation on the reflectivity spectrum is clearly seen by comparing the spectra before and after 90 min of light exposure (Figure 7b). As observed in **1** (Figure SI15c), a considerable change of the optical spectra is observed corresponding the photoinduced LS-to-HS spin-crossover of the $[Fe^{II}(LN_5)(CN)_2]$ moieties. Upon heating from 10 to 270 K (at 4 K/min; Figure 7a, green symbols), R_{750} is staying first stable until 30 K before rapidly increasing around 50 K as the system is relaxing into its initial thermodynamic LS state. Interestingly, this relaxation of the photoinduced HS species occurs at a much lower temperature for **3** than for **1** (50 K vs 120 K). This result might be the consequence of the elastic interactions between the SCO units created by the 1D coordination network. Overall, these optical properties demonstrate unambiguously that the intrinsic photoactivity of the $[Fe^{II}(LN_5)(CN)_2]$ unit is kept after coordinating the $\{Mn^{III}_2\}$ SMMs in **3**.

Additional photoexcitation experiments were made at selected wavelengths using LED sources. The optimal wavelength to photoinduce the HS state of the $[Fe^{II}(LN_5)(CN)_2]$ unit in **3** was determined by checking the efficiency of the different LEDs at 10 K following the same experimental protocol already used for **1** (vide supra). The relative reflectivity ΔR ($\Delta R = R_{after} - R_{before}$, Figure SI19a) reveals an efficient photoconversion in a broad spectral domain from 385 to 660 nm with an optimum wavelength around 590 nm (Figure SI19b). At this wavelength, the conversion is very efficient and rapid at least on the surface of the sample that is probed by this reflectivity technique. In about 10 min of exposure at 590 nm (P = 0.8 mW/cm^2), the optical reflectivity at 750 nm is saturated (Figure SI19c), and the Fe^{II} ions are fully converted in their HS state. It is worth noting that white light or 590-nm LED irradiations are qualitatively similar in terms of efficiency and that the thermal relaxation of the metastable HS state photoinduced by these different lights occurs at about the same temperature (50 K). Nevertheless, the time stability at 10 K of the photoinduced state (Figure SI20) is good over 30 min allowing the detailed study of the possible HS-to-LS photoreversibility with different wavelengths at 10 K. To test this photoreversibility of the spin-crossover in **3**, the HS state of the $[Fe^{II}(LN_5)(CN)_2]$ units was fully populated by a 590-nm irradiation during 15 min (P = 1.6 mW/cm^2) followed by a 15 min irradiation at particular wavelengths between 940 and 385 nm (P = 1.6 mW/cm^2). In contrast to complex **1**, the HS-to-LS photoreverse effect is very effective using LED sources between 735 and 940 nm with an optimum wavelength of 850 nm (Figure SI21a). As judged by the time evolution of R_{750} during a 850 nm irradiation (Figure SI21b), the HS-to-LS reverse photoconversion is saturated at the sample surface after about 20 min recovering about 85% of LS sites. As expected in this situation, the optical spectrum of **3** with LS $[Fe^{II}(LN_5)(CN)_2]$ units is qualitatively well recovered (Figure SI21c). Unsuccessful attempts were performed to test the possibility to improve the reversibility of the HS-to-LS photoconversion by increasing the 850-nm diode power up to 16 mW/cm^2. As shown in Figure 8, cycles of LS-to-HS and HS-to-LS photoconversions (using 590 and 850-nm irradiations, respectively) are perfectly reproducible allowing a good photoreversibility in **3**.

The impact on the magnetic properties of the light-induced spin-crossover of the $[Fe^{II}(LN_5)(CN)_2]$ units in **3** has been

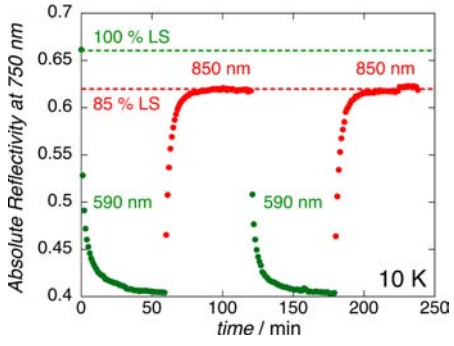

Figure 8. Time evolution of R_{750} for **3** during 2 cycles of LED irradiations at 590 ± 10 nm (60 min, P = 0.8 mW/cm^2, in green) and at 850 ± 10 nm (60 min, P = 4 mW/cm^2, in red). The dotted green line marks the R_{750} value at 10 K when the sample is cooled from room temperature in the dark.

dx.doi.org/10.1021/ja407570n | J. Am. Chem. Soc. 2013, 135, 14840−14853

studied by photomagnetic measurements. The sample was cooled to 5 K in the absence of light before being exposed to a green 539 nm light (P = 5 mW/cm^2) during 10 h (the time evolution of the χT product during the irradiation is given Figure SI22). At 5 K, the χT product of 3.8 cm^3 K/mol is remarkably decreased under irradiation at 539 nm until being close to saturation after about 10 h around 2.3 cm^3 K/mol. This magnetic behavior is unambiguously linked to the bulk photoinduced formation of HS Fe^{II} sites (S = 2) in **3** observed by surface optical reflectivity. At a first look, the decrease of the χT product at 5 K seems to be a counterintuitive result considering the formation of new magnetic centers. Nevertheless, these photoinduced S = 2 Fe^{II} centers are indeed linked and thus magnetically coupled, via the cyanido bridges to the S = 2 Mn^{III}/saltmen moieties. As observed in compound **2**, this Fe$^{II}_{HS}$–Mn$^{III}_{HS}$ interaction is expected to be antiferromagnetic (Figure 4) and thus to reduce the χT product at low temperatures. The signature of these antiferromagnetic interactions is clearly seen on the χT vs T data (in the dark) of the metastable photoinduced phase (green symbols Figure 9). The χT product increases from 1.23 at 1.8 K to 5.95 cm^3 K/mol at 40 K. Above this temperature, the photogenerated state relaxes, and the thermodynamic phase with LS Fe^{II} sites is fully recovered above 54 K as already observed by reflectivity measurements.

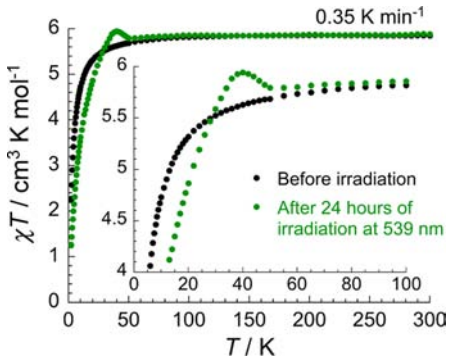

Figure 9. Temperature dependence of the χT product of **3** at 10000 Oe (at a temperature rate of 0.35 K min^{-1}) before (black symbols) and after a 24 h irradiation at 5 K (green symbols) with a green light (539 ± 10 nm, P = 5 mW/cm^2).

In order to estimate the percentage of photoconverted sites in the bulk sample of **3**, the magnetic susceptibility before and after photoirradiation was fitted to a Curie–Weiss law leading to the following Curie–Weiss constants: C = 6.0 and 7.7 cm^3 K mol^{-1} and θ = −2.9 and −11.3 K, respectively (Figure SI23). The comparison of the Curie–Weiss constants allows an estimation of the amount of Fe^{II} HS sites in **3** using eq 6:

$$\%_{HS} = \frac{C_{\text{after } h\nu} - C_{\text{before } h\nu}}{C_{\text{theoretical after } h\nu} - C_{\text{before } h\nu}} \quad (6)$$

Based on this expression and a theoretical Curie constant of 9.3 cm^3 K mol^{-1} (taking complex **2** as a reference), about 51% of the Fe^{II} sites are converted into HS species after a 24 h irradiation at 5 K with a 539-nm light. The amplitude of the exchange couplings along the chain cannot be determined as the photoconversion is only partial, but the increase of the Weiss constant upon the photogeneration of the HS [Fe^{II}(LN$_5$)(CN)$_2$] units clearly confirms the antiferromagnetic nature of the Fe$^{II}_{HS}$–Mn$^{III}_{HS}$ interaction as seen in **2**. It is worth mentioning that in contrast to **1**, a white light exposure of **3** does not allow an effective LS-to-HS photoconversion as no significant changes of the χT product were detected even after 18 h (Figure 10).

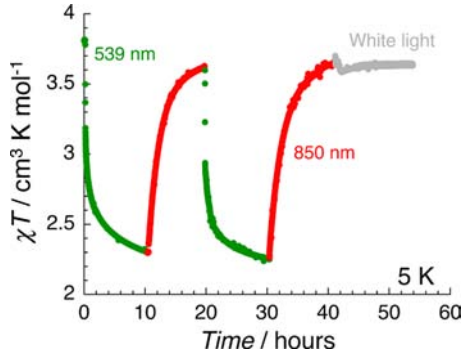

Figure 10. Time evolution of the χT product of **3** at 5 K during several cycles of excitation at 539 ± 10 nm (P = 5 mW/cm^2) during 10 h (green symbols) followed by de-excitation at 830 ± 10 nm (P = 0.55 mW/cm^2) during 10 h (red symbols) and finally after two cycles, an irradiation with a white light (P = 10 mW/cm^2) during 18 h (gray symbols).

As already observed by optical reflectivity on the sample surface (vide supra), the HS-to-LS photoreverse effect was tested on a bulk sample of **3** by photomagnetic measurements. At 5 K, the crystalline sample was first exposed during 10 h to a 539-nm green light (P = 5 mW/cm^2) to photoinduce the LS-to-HS spin-crossover of the Fe^{II} sites, and then a 850-nm light (P = 0.55 mW/cm^2) was used during also 10 h to reverse the process. During this sequence of irradiations, the magnetic susceptibility was measured as shown in Figure 10. Remarkably in comparison to **1** (Figure SI6b), 90% of the photogenerated HS Fe^{II} ions are reconverted in LS Fe^{II} ions under the 850-nm light exposure. Two cycles of successive 539/830 nm irradiations were performed highlighting the excellent reversibility and reproducibility of the photoinduced spin-crossover.

To conclude this paragraph on the optical and photomagnetic properties, it is important to emphasize that these experiments demonstrate that the photocontrolled properties of the LS [Fe(LN$_5$)(CN)$_2$] unit are preserved inside compound **3** and thus in a coordination network. This simple result was not straightforward as we observed previously that the association of the photochromic and photomagnetic [Fe(CN)$_5$(NO)]$^{2-}$ complex with Mn^{III} Schiff-base complexes resulted in new materials in which the intrinsic properties of the photoactive precursor are lost.[35] Moreover, compound **2** illustrates that the photoinduced optical and magnetic properties of the [Fe(LN$_5$)(CN)$_2$] unit can be completely lost if this building block crystallizes in a heptacoordinated geometry. Although a thermally and photoinduced spin-crossover has been already reported in several heterometallic coordination networks or complexes,[17,37] **3** is to the best of our knowledge the first 1D coordination network of SMMs bridged by spin-crossover units inducing thermally and photoreversible magnetic and optical properties. While the SMM behavior of the S_T = 4 {Mn$^{III}_2$} moiety in **3** has been established when the [Fe(LN$_5$)(CN)$_2$] unit is in its LS state (Figures 5 and 6), this property, or any other sign of slow relaxation of the magnetization, was not observed in the photoinduced phase containing a maximum amount of 51% of the HS [Fe(LN$_5$)-

dx.doi.org/10.1021/ja407570n | J. Am. Chem. Soc. 2013, 135, 14840–14853

$(CN)_2$] units. This result might be due to the weakness of the ac signal, difficult to detect with our photomagnetic setup, or simply due to the disappearance of the SMM properties suggesting that this property might be switched "on" and "off" by light depending of the spin state of the [$Fe(LN_5)(CN)_2$] units.

CONCLUSION

In this work, we reported for the first time the crystallographic structure of the spin-crossover [$Fe(LN_5)(CN)_2$]·H_2O (**1**) complex and a comprehensive study of its optical and photomagnetic properties in its crystalline form. This photomagnetic complex was successfully used as a coordinating linker of Mn^{III}/saltmen units affording a trinuclear species, [{Mn(saltmen)}$_2$$Fe(LN_5)(CN)_2$]$(ClO_4)_2$·0.5$CH_3OH$ (**2**), and a wave-shaped 1D coordination network of formula [{Mn(saltmen)}$_2${$Fe(LN_5)(CN)_2$}]$(ClO_4)_2$·0.5$C_4H_{10}O$·0.5H_2O (**3**) by controlling the addition order of the reagents. Addition of the Mn^{III}/Schiff-base precursor on [$Fe(LN_5)(CN)_2$] (**1**) leads to the connection of two [Mn(saltmen)]$^+$ units to each cyanido groups of **1** stabilizing the trinuclear species **2**, whereas the reverse addition order allows the conservation of the initial dinuclear Mn^{III}/Schiff-base units in **3** with a Mn/Fe 2:1 ratio. Both compounds were structurally characterized revealing that compound **3** can be seen as a 1D coordination polymer of **2**. Nevertheless, the Fe^{II} site in **2** and **3** has a different coordination sphere, hepta- vs hexa-coordinated, respectively, resulting in a different Fe^{II} spin state: S = 2 and 0, respectively. The spin state of the Fe^{II} center can be also straightforwardly forecasted using infrared spectroscopy or the crystal or reaction solution color. Complex **2** allowed us to estimate for the first time the Fe^{II}_{HS}−Mn^{III}_{HS} interaction through a cyanido bridge that appeared to be weak and of antiferromagnetic nature (J/k_B = −0.96(3) K). In **3**, dominant antiferromagnetic interactions were surprisingly found between Mn^{III} ions in one of the two crystallographically independent [Mn_2(saltmen)$_2$]$^{2+}$ moieties through the usual bisphenolato bridge, whereas ferromagnetic interactions were detected in the second one. On the other hand, the magnetic interaction through the LS [$Fe(LN_5)$-$(CN)_2$] linker between the two non equivalent {Mn_2} entities was found to be negligible above 1.8 K. The typical SMM properties (Δ_{eff}/k_B = 13.9 K) of the ferromagnetically coupled [Mn_2(saltmen)$_2$]$^{2+}$ unit in **3** were observed and studied by ac susceptibility measurements. Optical reflectivity and photomagnetic measurements revealed that the LS [$Fe(LN_5)(CN)_2$] unit in **3** can be efficiently converted in HS units under 660 to 385 nm light irradiations (with an optimum wavelength around 590 nm), while the reverse spin-crossover phenomenon is also accessible using 940 to 735 nm light exposures (with an optimum wavelength of 850 nm). In contrast to **1**, successive light irradiations proved the excellent reversibility and reproducibility of the photoinduced spin-crossover in **3** at low temperatures. To the best of our knowledge, compound **3** represents the initial demonstration of a coordination network of SMMs linked by spin-crossover units inducing thermally and photoreversible magnetic and optical properties. More generally, these results validate our rational building block synthetic approach assembling SCO and SMM precursors to design photoswitchable molecule-based magnetic materials in particular future SMMs, SCMs, or more generally magnets.

ASSOCIATED CONTENT

Supporting Information

Additional X-ray, optical and magnetic data and CIF files. This material is available free of charge via the Internet at http://pubs.acs.org.

AUTHOR INFORMATION

Corresponding Authors

clerac@crpp-bordeaux.cnrs.fr
celine.pichon@lcc-toulouse.fr
mathon@icmcb-bordeaux.cnrs.fr

Present Addresses

[⊥]LCC, CNRS and Université de Toulouse (UPS, INP), 205 route de Narbonne, 31077 Toulouse, France.
[▽]Key Laboratory of Polyoxometalate Science of Ministry of Education, Faculty of Chemistry, Northeast Normal University, Ren Min Street no. 5268, Changchun, Jilin 130024, P. R. China.

Notes

The authors declare no competing financial interest.

ACKNOWLEDGMENTS

This work was supported by the University of Bordeaux, the CNRS, the Aquitaine Région, the IUF (Institut Universitaire de France) and the ANR (NT-09_469563, AC-MAGnets project). The authors would like to thank P. Merzeau, M. Rouzières, M. Kalisz, G. Godillot, N. Hearns, E. Lebraud, C. Sinito, P. Négrier, X. Liu, C. Coulon, and H. Miyasaka for their technical assistance and fruitful discussions.

REFERENCES

(1) (a) Kahn, O.; Martinez, C. J. *Science* **1998**, *279*, 44. (b) Bousseksou, A.; Molnár, G.; Salmon, L.; Nicolazzi, W. *Chem. Soc. Rev.* **2011**, *40*, 3313. (c) *Magnetism: Molecules to Materials*; Miller, J. S., Drillon, M., Eds.; Wiley-VCH: Weinheim, 2002; Vols. *I*−*V* and references within. (d) Sato, O.; Tao, J.; Zhang, Y.-Z. *Angew. Chem., Int. Ed.* **2007**, *46*, 2152 and references within. (e) Freedman, D. E.; Jenkins, D. M.; Iavarone, A. T.; Long, J. R. *J. Am. Chem. Soc.* **2008**, *130*, 2884. (f) Dul, M. C.; Parod, E.; Lescouëzec, R.; Chamoreau, L. M.; Villain, F.; Journaux, Y.; Ruiz-García, R.; Cano, J.; Julve, M.; Lloret, F.; Pasan, J.; Ruiz-Pérez, C. *J. Am. Chem. Soc.* **2009**, *131*, 14614. (g) McConnell, A. C.; Bell, J. D.; Miller, J. S. *Inorg. Chem.* **2012**, *51*, 9978. (h) Muñoz-Lara, F. J.; Arcís-Castillo, Z.; Muñoz, M. C.; Rodríguez-Velamazán, J. A.; Gaspar, A. B.; Real, J. A. *Inorg. Chem.* **2012**, *51*, 11126. (i) *Spin-Crossover Materials: Properties and Applications*; Halcrow, M. A., Ed.; Wiley-VCH: Weinheim, 2013.

(2) (a) Létard, J.-F.; Guionneau, P.; Goux-Capes, L. *Top. Curr. Chem.* **2004**, *235*, 221 and references within. (b) Gatteschi, D.; Sessoli, R.; Villain, J. *Molecular Nanomagnets*; Oxford University Press: New York, 2006 and references within. (c) Wäckerlin, C.; Chylarecka, D.; Kleibert, A.; Müller, K.; Iacovita, C.; Nolting, F.; Jung, T. A.; Ballav, N. *Nat. Commun.* **2010**, *1*, 61. (d) Venkataramani, S.; Jana, U.; Dommaschk, M.; Sönnichsen, F. D.; Tuczek, F.; Herges, R. *Science* **2011**, *331*, 445.

(3) (a) *Molecular Materials*, Bruce, D. W., O'Hare, D., Walton, R. I., Eds.; Wiley & Sons: Hoboken, 2010 and references within. (b) *Multifunctional Molecular Materials*; Ouahab, L., Ed.; Pan Stanford Publishing Pte Ltd: Singapore, 2013 and references within.

(4) (a) Sessoli, R.; Tsai, H.-L.; Schake, A. R.; Wang, S.; Vincent, J. B.; Folting, K.; Gatteschi, D.; Christou, G.; Hendrickson, D. N. *J. Am. Chem. Soc.* **1993**, *115*, 1804. (b) Sessoli, R.; Gatteschi, D.; Caneschi, A.; Novak, M. A. *Nature* **1993**, *365*, 141. (c) Christou, G.; Gatteschi, D.; Hendrickson, D. N.; Sessoli, R. *MRS Bull.* **2000**, *25*, 66. (d) Gatteschi, D.; Sessoli, R. *Angew. Chem., Int. Ed.* **2003**, *42*, 268. (e) *Single-Molecule Magnets and Related Phenomena*; Winpenny, R., Ed.; Springer: New York, 2006; Vol. *122* and references within.

(5) (a) Caneschi, A.; Gatteschi, D.; Lalioti, N.; Sangregorio, C.; Sessoli, R.; Venturi, G.; Vindigni, A.; Rettori, A.; Pini, M. G.; Novak, M. A. *Angew. Chem., Int. Ed.* **2001**, *40*, 1760. (b) Clérac, R.; Miyasaka, H.; Yamashita, M.; Coulon, C. *J. Am. Chem. Soc.* **2002**, *124*, 12837.
(6) Coulon, C.; Miyasaka, H.; Clérac, R. *Struct. Bonding (Berlin)* **2006**, *122*, 163.
(7) (a) Leuenberger, M. N.; Loss, D. *Nature* **2001**, *410*, 789. (b) Cavallini, M.; Gomez-Segura, J.; Ruiz-Molina, D.; Massi, M.; Albonetti, C.; Rovira, C.; Veciana, J.; Biscarini, F. *Angew. Chem., Int. Ed.* **2005**, *44*, 888. (c) Bogani, L.; Wernsdorfer, W. *Nat. Mater.* **2008**, *7*, 179.
(8) (a) Roubeau, O.; Clérac, R. *Eur. J. Inorg. Chem.* **2008**, *28*, 4325. (b) Ferbinteanu, M.; Miyasaka, H.; Wernsdorfer, W.; Nakata, K.; Sugiura, K.-i.; Yamashita, M.; Coulon, C.; Clérac, R. *J. Am. Chem. Soc.* **2005**, *127*, 3090. (c) Coulon, C.; Clérac, R.; Wernsdorfer, W.; Colin, T.; Miyasaka, H. *Phys. Rev. Lett.* **2009**, *102*, 167204. (d) Miyasaka, H.; Takayama, K.; Saitoh, A.; Furukawa, S.; Yamashita, M.; Clérac, R. *Chem.—Eur. J.* **2010**, *16*, 3656. (e) Jeon, I.-R.; Clérac, R. *Dalton Trans.* **2012**, *41*, 9569.
(9) Wernsdorfer, W.; Aliaga-Alcalde, N.; Hendrickson, D. N.; Christou, G. *Nature* **2002**, *416*, 406.
(10) (a) Wernsdorfer, W.; Bhaduri, S.; Tiron, R.; Hendrickson, D. N.; Christou, G. *Phys. Rev. Lett.* **2002**, *89*, 197201. (b) Tiron, R.; Wernsdorfer, W.; Aliaga-Alcade, N.; Christou, G. *Phys. Rev. B* **2003**, *68*, 140407. (c) Wernsdorfer, W.; Bhaduri, S.; Vinslava, A.; Christou, G. *Phys. Rev. B* **2005**, *72*, 214429.
(11) Miyasaka, H.; Madanbashi, T.; Sugimoto, K.; Nakazawa, Y.; Wernsdorfer, W.; Sugiura, K.-i.; Yamashita, M.; Coulon, C.; Clérac, R. *Chem.—Eur. J.* **2006**, *12*, 7028.
(12) (a) Miyasaka, H.; Clérac, C.; Mizushima, K.; Sugiura, K.-i.; Yamashita, M.; Wernsdorfer, W.; Coulon, C. *Inorg. Chem.* **2003**, *42*, 8203. (b) Coulon, C.; Clérac, R.; Lecren, L.; Wernsdorfer, W.; Miyasaka, H. *Phys. Rev. B* **2004**, *69*, 132408. (c) Miyasaka, H.; Nezu, T.; Sugimoto, K.; Sugiura, K.-i.; Yamashita, M.; Clérac, R. *Chem.—Eur. J.* **2005**, *11*, 1592. (d) Miyasaka, H.; Saitoh, A.; Yamashita, M.; Clérac, R. *Dalton Trans.* **2008**, 2422.
(13) (a) Hauser, A.; Jeftic, J.; Romstedt, H.; Hinek, R.; Spiering, H. *Coord. Chem. Rev.* **1999**, *190–192*, 471. (b) Gütlich, P.; Garcia, Y.; Goodwin, H. A. *Chem. Soc. Rev.* **2000**, *29*, 419. (c) Real, J. A.; Gaspar, A. B.; Niel, V.; Muñoz, M. C. *Coord. Chem. Rev.* **2003**, *236*, 121. (d) *Spin Crossover in Transition Metal Compounds*; Gütlich, P., Goodwin, H. A., Eds.; Topics in Current Chemistry; Springer: Berlin, 2004; Vol. *1*.
(14) (a) Decurtins, S.; Gütlich, P.; Köhler, C. P.; Spiering, H.; Hauser, A. *Chem. Phys. Lett.* **1984**, *105*, 1. (b) Decurtins, S.; Gütlich, P.; Hasselbach, K. M.; Hauser, A.; Spiering, H. *Inorg. Chem.* **1985**, *24*, 2174. (c) Gütlich, P.; Garcia, Y.; Woike, T. *Coord. Chem. Rev.* **2001**, *219–221*, 839 and references within. (d) Létard, J.-F. *J. Mater. Chem.* **2006**, *16*, 2550.
(15) (a) Miyasaka, H.; Clérac, R.; Ishii, T.; Chang, H.-C.; Kitagawa, S.; Yamashita, M. *J. Chem. Soc., Dalton Trans.* **2002**, 1528. (b) Miyasaka, H.; Clérac, R.; Wernsdorfer, W.; Lecren, L.; Bonhomme, C.; Sugiura, K.-i.; Yamashita, M. *Angew. Chem., Int. Ed.* **2004**, *43*, 2801.
(16) (a) Nelson, S. A.; McIlroy, P. D. A.; Stevenson, C. S.; König, E.; Ritter, G.; Waigel, J. *J. Chem. Soc., Dalton Trans.* **1986**, 991. (b) König, E.; Ritter, G.; Dengler, J.; Nelson, S. M. *Inorg. Chem.* **1987**, *26*, 3582. (c) Sánchez-Costa, J. Ph. D. Thesis, University of Bordeaux, France, 2005.
(17) (a) Hayami, S.; Gu, Z.; Einaga, Y.; Fujishima, A.; Sato, O. *Mol. Cryst. Liq. Cryst.* **2000**, *343*, 65. (b) Hayami, S.; Juhász, G.; Maeda, Y.; Yokoyama, T.; Sato, O. *Inorg. Chem.* **2005**, *44*, 7289.
(18) Zhang, Y.-Z.; Wang, B.-W.; Sato, O.; Gao, S. *Chem. Commun.* **2010**, *46*, 6959.
(19) Venkatakrishnan, T. S.; Sahoo, S.; Bréfuel, N.; Duhayon, C.; Paulsen, C.; Barra, A.-L.; Ramasesha, S.; Sutter, J.-P. *J. Am. Chem. Soc.* **2010**, *132*, 6047.
(20) Wang, Q.-L.; Southerland, H.; Li, J.-R.; Prosvirin, A. V.; Zhao, H.; Dunbar, K. R. *Angew. Chem., Int. Ed.* **2012**, *51*, 9321.
(21) (a) Dong, D.-P.; Liu, T.; Kanegawa, S.; Kang, S.; Sato, O.; He, C.; Duan, C.-Y. *Angew. Chem., Int. Ed.* **2012**, *51*, 5119. (b) Morimoto, M.; Miyasaka, H.; Yamashita, M.; Irie, M. *J. Am. Chem. Soc.* **2009**, *131*, 9823. (c) Hoshino, N.; Iijima, F.; Newton, G. N.; Yoshida, N.; Shiga, T.; Nojiri, H.; Nakao, A.; Kumai, R.; Murakami, Y.; Oshio, H. *Nat. Chem.* **2012**, *4*, 921.
(22) Otwinowski, Z.; Minor, W. *Methods Enzymol.* **1996**, *276*, 307.
(23) Sheldrick, G. M. *SHELXL-97*; Program for Crystal Structure Refinement, University of Göttingen, 1997.
(24) **1** could also be crystallized with diethyl ether vapor diffusion in dimethylformamide leading to $[Fe(LN_5)(CN)_2]\cdot 0.5H_2O$: $[Fe(LN_5)(CN)_2]\cdot H_2O$ (200 mg, 0.53 mmol) was dissolved in DMF (30 mL) and stirred for 3 h. Insoluble material was removed by filtration. Small cubic crystals were obtained after one night by diffusion of the pink violet solution with diethyl ether. Crystal yield: 6 mg (3%). IR data (KBr, cm^{-1}): $\nu(OH_w)$ 3514 (s), ν(NH) 3317 (m), $\nu(C{\equiv}N)$ 2087 (s), $\nu(C{=}N)$ 1616 (s). Due to the low yield, an elemental analysis was not done. Unit cell parameters: a = 7.643(1) Å, b = 23.561(5) Å, c = 10.144(3) Å, β = 102.9(1)°, V = 1820.0(7) $Å^3$.
(25) For example: (a) Kunkeler, P. J.; van Koningsbruggen, P. J.; Cornelissen, J. P; van der Horst, A. N.; van der Kraan, A. M.; Spek, A. L.; Haasnoot, J. G.; Reedjik, J. *J. Am. Chem. Soc.* **1996**, *118*, 2190. (b) Molnár, G.; Niel, V.; Gaspar, A. B.; Real, J.-A.; Zwick, A.; Bousseksou, A.; McGarvey, J. J. *J. Phys. Chem. B* **2002**, *106*, 9701.
(26) Guionneau, P.; Le Gac, F.; Kaiba, A.; Sánchez Costa, J.; Chasseau, D.; Létard, J.-F. *Chem. Commun.* **2007**, 3723.
(27) Guionneau, P.; Sánchez Costa, J.; Létard, J.-F. *Acta Cryst. C* **2004**, *60*, m587.
(28) Sánchez-Costa, J.; Balde, C.; Carbonera, C.; Denux, D.; Wattiaux, A.; Desplanches, C.; Ader, J.-P.; Gütlich, P.; Létard, J.-F. *Inorg. Chem.* **2007**, *46*, 4114.
(29) (a) van Vleck, J. H. *The Theory of Electric and Magnetic Susceptibility*; Oxford University Press: London, 1932. (b) O'Connor, C. J. *Prog. Inorg. Chem.* **1982**, *29*, 203.
(30) Shyu, H.-L.; Wei, H.-H.; Wang, Y. *Inorg. Chim. Acta* **1999**, *290*, 8.
(31) (a) Kennedy, B. J.; Murray, K. *Inorg. Chem.* **1985**, *24*, 1552. (b) Matsumoto, N.; Zhong, Z. J.; Okawa, H.; Kida, S. *Inorg. Chim. Acta* **1989**, *160*, 153. (c) Bermejo, M. R.; Castiñeiras, A.; Garcia-Monteagudo, J. C.; Rey, M.; Sousa, A.; Watkinson, M.; McAuliffe, C. A.; Pritchard, R. G.; Beddoes, R. L. *J. Chem. Soc., Dalton Trans.* **1996**, 2935.
(32) (a) Matsumoto, N.; Zhong, Z. J.; Okawa, H.; Kida, S. *Inorg. Chim. Acta* **1989**, *160*, 153. (b) Lecren, L.; Wernsdorfer, W.; Li, Y.-G.; Vindigni, A.; Miyasaka, H.; Clérac, R. *J. Am. Chem. Soc.* **2007**, *129*, 5045. (c) Wu, Q.; Li, Y.-G.; Wang, Y.-H.; Clérac, R.; Lu, Y.; Wang, E.-B. *Chem. Commun.* **2009**, 5743. (d) Mandal, S.; Rout, A. K.; Fleck, M.; Pilet, G.; Ribas, J.; Bandyopadhyay, D. *Inorg. Chim. Acta* **2010**, *363*, 2250. (e) Sawada, Y.; Kosaka, W.; Hayashi, Y.; Miyasaka, H. *Inorg. Chem.* **2012**, *51*, 4824. (f) Miyasaka, H.; Saitoh, A.; Nakano, M. *Dalton Trans.* **2012**, *41*, 13691.
(33) Fisher, M. E. *Am. J. Phys.* **1964**, *32*, 343.
(34) Ge, C.-H.; Cui, A.-L.; Ni, Z.-H.; Jiang, Y.-B.; Zhang, L.-F.; Ribas, J.; Kou, H.-Z. *Inorg. Chem.* **2006**, *45*, 4883.
(35) Ababei, R.; Li, Y.-G.; Roubeau, O.; Kalisz, M.; Bréfuel, N.; Coulon, C.; Harté, E.; Liu, X.; Mathonière, C.; Clérac, R. *New J. Chem.* **2009**, *33*, 1237.
(36) (a) Hayami, S.; Gu, Z.-Z.; Einaga, Y.; Kobayasi, Y.; Ishikawa, Y.; Yamada, Y.; Fujishima, A.; Sato, O. *Inorg. Chem.* **2001**, *40*, 3240. (b) Liu, H.; Fujishima, A.; Sato, O. *Appl. Phys. Lett.* **2004**, *85*, 2295.
(37) (a) Niel, V.; Thompson, A. L.; Goeta, A. E.; Enachescu, C.; Hauser, A.; Galet, A.; Munoz, M. C.; Real, J. A. *Chem.—Eur. J.* **2005**, *11*, 2047. (b) Papanikolaou, D.; Margadonna, S.; Kosaka, W.; Ohkoshi, S.-i.; Brunelli, M.; Prassides, K. *J. Am. Chem. Soc.* **2006**, *128*, 8358. (c) Agustí, G.; Cobo, S.; Gaspar, A. B.; Molnar, G.; Moussa, N. O.; Szilagyi, P. Á.; Palfi, V.; Vieu, C.; Muñoz, M. C.; Real, J. A.; Bousseksou, A. *Chem. Mater.* **2008**, *20*, 6721. (d) Agustí, G.; Thompson, A. L.; Gaspar, A. B.; Muñoz, M. C.; Goeta, A. E.; Rodríguez-Velamázan, J. A.; Castro, M.; Burriel, R.; Real, J. A. *Dalton*

Trans. **2008**, 642. (e) Seredyuk, M.; Gaspar, A. B.; Ksenofontov, V.; Verdaguer, M.; Villain, F.; Gütlich, P. *Inorg. Chem.* **2009**, *48*, 6130. (f) Rodríguez-Velamázan, J. A.; Carbonera, C.; Castro, M.; Palacios, E.; Kitazawa, T.; Létard, J.-F.; Burriel, R. *Chem.—Eur. J.* **2010**, *16*, 8785. (g) Muñoz, M. C.; Real, J. A. *Coord. Chem. Rev.* **2011**, *255*, 2068. (h) Funck, K. E.; Prosvirin, A. V.; Mathonière, C.; Clérac, R.; Dunbar, K. R. *Inorg. Chem.* **2011**, *50*, 2782. (i) Ohkoshi, S.-i.; Imoto, K.; Tsunobuchi, Y.; Takano, S.; Tokoro, H. *Nature Chem.* **2011**, *3*, 564. (j) Sciortino, N. F.; Scherl-Gruenwald, K. R.; Chastanet, G.; Halder, G. J.; Chapman, K. W.; Létard, J.-F.; Kepert, C. J. *Angew. Chem., Int. Ed.* **2012**, *51*, 10154. (k) Martínez, V.; Castillo, Z. A.; Muñoz, M. C.; Gaspar, A. B.; Etrillard, C.; Létard, J.-F.; Terekhov, S. A.; Bukin, G. V.; Levchenko, G.; Real, J. A. *Eur. J. Inorg. Chem.* **2013**, *5*, 813.